NUMERICAL MODELLING OF CFRP SHEETS EXTERNALLY BONDED TO REINFORCED CONCRETE

by

Adam John Lawlor

B.Sc.E. (Civil Engineering), University of New Brunswick, 2016

A Report Submitted in Partial Fulfillment
of the Requirements for the Degree of

Master of Engineering

in the Graduate Academic Unit of Civil Engineering

Supervisor: Alan Lloyd, PhD, PEng., Department of Civil Engineering

Examining Board: Kaveh Arjomandi, PhD, PEng., Department of Civil Engineering
Othman Nasir, PhD, PEng., Department of Civil Engineering

This report is accepted by the Dean of Graduate Studies

THE UNIVERSITY OF NEW BRUNSWICK

August, 2020

ABSTRACT

Fibre reinforced polymers (FRP) are becoming a commonly used material in retrofitting and rehabilitating deteriorating concrete structures. Aside from its high strength, FRP is a lightweight, non-corrosive, and relatively cheap alternative to traditional rehabilitation methods. One of the major components of FRP externally bonded to reinforced concrete is the bond and its behaviour at the FRP-concrete interface. Previous studies have investigated debonding of FRP sheets externally bonded to reinforced concrete through experimental testing as well as finite element modelling. This project presents the numerical modelling of CFRP sheets externally bonded to reinforced concrete. Using the finite element analysis software ABAQUS, three specimens of varying bond lengths subjected to double lap shear were modelled and analyzed. The results were discussed and compared to an experimental study previously performed.

ACKNOWLEDGEMENTS

I would like to express my gratitude and appreciation to my supervisor Dr. Alan Lloyd, for his help, guidance, and patience working around my work schedule throughout the pursuit of this degree. I would like to thank my family for their endless support since I began my university career. To my best friend, partner-in-crime, and soon to be wife, Katie: I cannot express the amount of appreciation, gratitude, and love I have for you. Thank you for your continual support and encouragement, your unwavering love, and your patience when listening to my (very) long rants about school, work, and everything else throughout this entire process. You are my whole heart. I would also like to thank my precious dog Maisy, for bringing joy in my life when needed the most. And finally, to my mother, whose courage, inspiration, and love, is present with me each and every day. You will always be my hero.

TABLE OF CONTENTS

LIST OF TABLES

LIST OF FIGURES

1.0 INTRODUCTION

1.1 Background

In today's era, concrete structures are deteriorating at an increasingly rapid rate. It is starting to become more commonplace to see concrete infrastructure, such as buildings and bridges, in a failing or near failing state. Firstly, the rapid deterioration can be attributed to the age of the structures. With the rapid economic growth and expansion after the second World War, it is becoming apparent within municipalities that parts of their infrastructure assets are reaching their end of design life. Municipalities are being faced with the decision on whether to improve the service life through rehabilitation or simply construct new. Aside from their age, concrete structures built several years ago were done so to a much different standard than today. These structures were designed to handle lower loads and capacity. Traditional rehabilitation methods on concrete structures involved using externally bonded steel plates. Steel sheets provide an attractive solution to strengthen and repair reinforced concrete due to its low cost and ease of construction, application, and maintenance [1]. Steel corrosion, however, is a major disadvantage of steel plates and is the main reason the industry is shifting to an alternative.

A fibre reinforced polymer (FRP) is a composite material that consists of a polymer matrix reinforced with fibres [2]. The most common of these materials are glass, carbon, and aramid. Other less common types of FRP's include basalt, wood, aluminum, and steel. Depending on its intended use, each different FRP material has its advantages and disadvantages. It can also be used in a variety of different applications such as bars, sheets, plates, and tendons. Aside from its relatively low cost, FRP is a lightweight, high strength, and non-corrosive material. It has a variety of uses, which range from the aircraft, marine, and automobile industry to the construction industry [2]. FRP's use in capacity strengthening and rehabilitation is relatively new in the industry, therefore there is continuous development in this field on its properties, proper usage, and maintenance.

For the purpose of this research project, carbon FRP (CFRP) sheets and their use as external reinforcement will be investigated. In order to properly design and apply CFRP as an external strengthening system, a thorough understand of three major components is necessary. This includes the CFRP sheet itself, the polymer (resin), and the substrate it is adhering to. The polymer, also known as the resin or epoxy, is essentially the glue that holds the fibres together as well as the sheet to the actual substrate (i.e concrete) as well. As discussed by many researchers, the interface between the CFRP sheet and concrete is most commonly the weakest part, therefore it plays the most crucial role [3]. An improperly applied resin will be ineffective in allowing the CFRP to reach its maximum strength capacity, thus resulting in an underutilized sheet.

When analyzing CFRP sheets externally bonded to reinforced concrete, researchers have found that the most common failure mode is debonding. Since CFRP is a very brittle material, having a thorough understanding of the bond of the CFRP-concrete interface as well as the ability to detect debonding failure is crucial in terms of safety [4]. While experimental testing conducted of CFRP strengthened reinforced concrete beams plays an important role in developing an understanding of debonding failure, there are many aspects that cannot be understood by testing alone [5]. By utilizing a finite element analysis software to model CFRP-concrete specimens, researchers can capture a more detailed numerical model of the specimen. More specifically, finite element modelling will provide a more thorough breakdown of the bond between the CFRP and concrete through each interval as it reaches its debonding failure.

1.2 Aims and Objectives

The aim of this project is to gain a more in-depth understanding of the bond between CFRP sheets externally bonded to reinforced concrete members subjected to static loading through the use of finite element analysis software. This project will examine the bond at the CFRP-concrete interface at a level beyond experimental testing. The work performed in this project is a continuation of a more extensive experimental study conducted on CFRP sheets externally bonded to reinforced concrete under static loading.

The main objectives of this project are presented as follows:

- Develop a better understanding of the bond between CFRP sheets and reinforced concrete members;
- Review experimental studies and numerical models previously conducted on CFRP sheets and reinforced concrete members subjected to static loading;
- Use finite element analysis software to simulate the experimental results conducted from the previous experimental study;
- Examine the effects of bond length on development length;
- Examine the failure mode, and;
- Determine the effects of different parameters and bond lengths on the reinforced concrete member, CFRP sheet, and their bond.

1.3 Scope of Work

The scope of this project involves the numerical modelling of CFRP sheets externally bonded to reinforced concrete. Furthermore, the previous experimental study will be discussed and compared to the finite model. The following list outlines the scope of work to be conducted for this project.

- Review previously conducted experimental studies and numerical models on the bond between CFRP and reinforced concrete, including the study to which this project is the continuation of;
- Review finite element analysis models of reinforced concrete, FRP materials, and cohesive materials;
- Simulate a finite element model of CFRP sheets externally bonded to reinforced concrete, replicating the setup of the previously conducted experimental study;
- Evaluate the model outputs. This will also include iterating different parameters, properties, and constraints to provide the most realistic and representative results;
- Compare the results from the finite element model to the experimental study in order to determine the model's level of accuracy;
- Outline and discuss the model's results; and,
- Summarize concluding remarks and provide design recommendations for future research.

1.4 Report Overview

This report encompasses seven (7) chapters. With a brief introduction and background outlined in the first chapter, a literature review is discussed in Chapter 2. This includes an investigation into fibre reinforced polymers and their varying types, along with an outline of their advantages and disadvantages when incorporating them. Furthermore, a literature search of several finite element analyses on FRP and reinforced concrete is conducted. Chapter 3 provides an overview to the more extensive experimental study conducted on CFRP sheets externally bonded to reinforced concrete under static loading. The numerical modelling and the use of finite element analysis will be discussed in Chapter 4, outlining commonly used finite element software as well as modelling techniques. Chapter 5 summarizes the construction of the finite element model. More specially, materials properties, inputs, parameters, and assumptions made throughout the model construction project will be discussed. Chapter 6 will outline the results from the finite element models, with a comparison conducted with the experimental results. Conclusions, modelling limitations, and recommendations regarding the project and future work will be presented in seventh and final the final chapter.

2.0 LITERATURE REVIEW

2.1 General

The different methods and means of conducting structure rehabilitation is becoming an increasingly popular topic in the industry. This can be attributed to a variety of different factors, such as increasing costs, design criteria, and age of existing infrastructure. With the rising costs of materials, labour, and tariffs, the construction field is beginning to shift towards modern and innovative rehabilitation methods to offset costs. The industry is no longer investing a lot in the more common and traditional methods due to high costs and poor service life. Furthermore, the level of required capacity on structures is steadily increasing due to many different aspects, such as newly developed standards for design along with environmental factors due to changing climate. With an increasing number of permitting and heavy haul vehicles, along with the rise in intensity of earthquakes, hurricanes, and other significantly damaging storms, the structural capacity is becoming increasingly difficult to reach and even more difficult to maintain. Therefore, it is becoming imperative to develop effective rehabilitation methods and techniques to meet these requirements, as the traditional methods are no longer as feasible as they once were.

With an aging infrastructure, complete replacement of all deteriorating structural assets is ideal but not a realistic option. Implementing fibre reinforced polymers (FRP), for example, is one of the many solutions that is being researched for proper rehabilitation at an economically sound cost. Many advantages of FRP aside from its inexpensiveness include its lightweight and ease of constructability, corrosive resistant properties, and high strength

[6]. Although it is becoming popular, there still exists room for improvement in terms of research and properly understanding the material.

The following sections outline some of traditional rehabilitation methods used in the industry with a brief look as to why they are becoming obsolete. Furthermore, the different types of commonly used FRPs will be discussed along with their fabrication process. The specific properties and material behaviour of fibre reinforced polymer will be addressed, as well as their common uses. Previously conducted experimental and numerical studies will also be touched on, along with studies involving finite element analysis models.

2.2 Traditional & Emerging Rehabilitation Methods

With the extreme degradation effects of harsh, climatic environments, developing innovative rehabilitating materials and methods is focusing more on reinforced concrete and masonry structures [7]. Prior to the development and implementation of these new materials, steel sheets and plates have been the traditional method of concrete rehab. Although steel has a very high strength and is commonly used for many designs, it is not an ideal material in every scenario. As explained by Carvajal et al. [8], corrosion of steel, specifically reinforcement, is the defining cause of degradation in concrete structures. Corrosion will often lead to longitudinal cracking of the concrete, a reduction of the steel reinforcement area, and deterioration of the bond between the rebar and concrete [8]. Unless the corrosion issue is completely resolved, using steel sheets or plates on a corrosive prone, degrading structure is quite counter intuitive. Oftentimes these corrosion issues can be difficult and costly to solve, as they are typically a result of a poor design or environmental factor. It is an expensive solution for a problem that will only be resolved temporarily.

Some of the newer developing rehabilitation methods, along with FRPs, include using materials such as fiberglass, aluminum, stainless steel, and ultra-high performing concrete. Concrete confinement, typically performed with one of the materials listed above, is also becoming a popular option. Previously conducted research shows that rehabilitating damaged concrete structures with external confinement is an effective solution in restoring the concrete's capacity [9].

Figure 2.1. Brick Column Reinforcement Through Steel Jacketing [10]

Different methods of concrete confinement include steel jacketing, concrete jacketing, and FRP jacketing to name a few. As discussed by ACI Committee 440 [11], concrete confinement can be used to increase its strength in axial compression as well as its ductility.

This can be demonstrated in Figure 2.2, which outlines a stress-strain curve comparison of a reinforced concrete column with varying confinement levels.

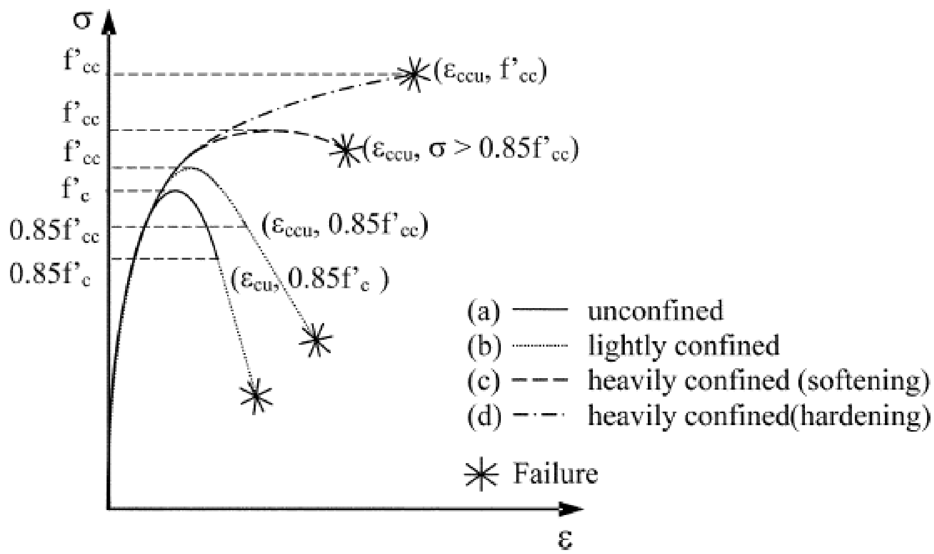

Figure 2.2. Stress-Strain Curve of Unconfined & Confined Concrete Columns [11]

2.3 Fibre Reinforced Polymers

Fibre reinforced polymers is a composite material that consists of two different materials: fibres and polymers. The fibres within FRP can consist of many different materials, which display varying material properties. Some of the more common FRP composites include carbon, glass, steel, aramid, and basalt. Due to their varying material properties, each type of FRP has different strengths and weaknesses in its application. Mechanical properties of some of the more common FRP types can be found in the following table.

Table 2.1. Mechanical Properties of Different FRP [12]

Property	Symbol	Units	Glass/ epoxy	Boron/ epoxy	Graphite/ epoxy
Fiber volume fraction	V_f		0.45	0.50	0.70
Longitudinal elastic modulus	E_1	GPa	38.6	204	181
Transverse elastic modulus	E_2	GPa	8.27	18.50	10.30
Major Poisson's ratio	ν_{12}		0.26	0.23	0.28
Shear modulus	G_{12}	GPa	4.14	5.59	7.17
Ultimate longitudinal tensile strength	$(\sigma_1^T)_{ult}$	MPa	1062	1260	1500
Ultimate longitudinal compressive strength	$(\sigma_1^C)_{ult}$	MPa	610	2500	1500
Ultimate transverse tensile strength	$(\sigma_2^T)_{ult}$	MPa	31	61	40
Ultimate transverse compressive strength	$(\sigma_2^C)_{ult}$	MPa	118	202	246
Ultimate in-plane shear strength	$(\tau_{12})_{ult}$	MPa	72	67	68
Longitudinal coefficient of thermal expansion	α_1	μm/m/°C	8.6	6.1	0.02
Transverse coefficient of thermal expansion	α_2	μm/m/°C	22.1	30.3	22.5
Longitudinal coefficient of moisture expansion	β_1	m/m/kg/kg	0.00	0.00	0.00
Transverse coefficient of moisture expansion	β_2	m/m/kg/kg	0.60	0.60	0.60

Source: Tsai, S.W. and Hahn, H.T., *Introduction to Composite Materials*, CRC Press, Boca Raton, FL, Table 1.7, p. 19; Table 7.1, p. 292; Table 8.3, p. 344. Reprinted with permission.

Carbon FRP

Carbon FRP (CFRP) is one of the two most commonly used composite FRP materials. With the steady incline of research into the field of FRP, CFRP sheets and plates are viewed as one of the most promising types of materials used in strengthening and rehabilitating reinforced concrete structures [13]. One of the more prominent reasons behind this is due to its resistant to corrosion as well as other deterioration experienced by harsh environmental conditions [6]. CFRP also has a very high elastic modulus, comparable to that of steel. In comparison to the other types of FRP however, CFRP can be costly but still remains a cheaper alternative to steel.

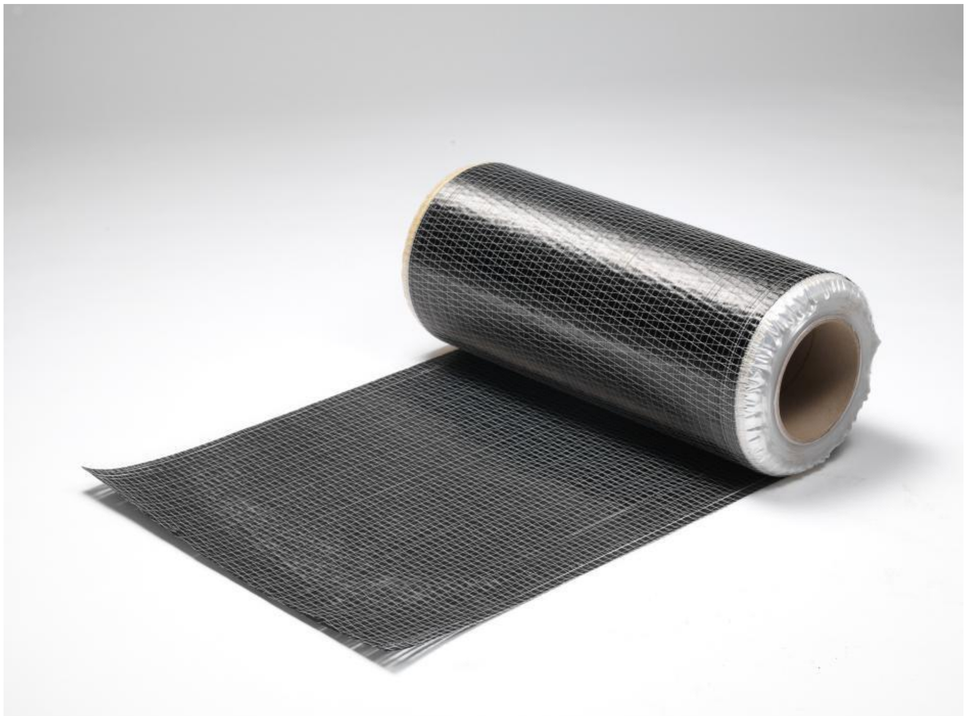

Figure 2.3. Roll of CFRP Sheet [14]

Glass FRP

Glass FRP (GFRP) is the other most commonly used FRP, next to carbon. Unlike carbon, GFRP is typically utilized in a bar form as an alternative to the traditional steel rebar. While they maintain a relatively low cost and are considered a high strength material, GFRP is limiting with their susceptibility to degradation in an alkaline environment [15]. They are, however, non-corrosive and provide an acceptable replacement to non-prestressed steel reinforcement. One of the more common difficulties in dealing with GFRP bars in the industry is its in-situ rehabilitation. Due to its brittleness and material behaviour, GFRP bars are difficult to strengthen, repair, and rehabilitation as they need a substantial bar lap length. This can hard to deal with in areas of limited space and cover.

Figure 2.4. GFRP Reinforcing Bar [16]

Although most commonly used as rebar, GFRP can still be fabricated in sheet form to provide external reinforcement, as shown in Figure 2.5.

Figure 2.5. Roll of CFRP Sheet [14]

Aramid FRP

Although less common than carbon and glass FRP, aramid FRP (AFRP) is still used around the world in rehabilitating structures. Similar to CFRP, AFRP is commonly used as a confinement sheet. When compared to the other types however, AFRP does have some advantages while sharing similarities. The use of AFRP sheets offer major benefits in the industry as it has improved ductile behaviour when compared to the other FRP types [17]. In certain situations, having a more ductile material such as aramid is a huge advantage, as FRP's brittleness is one of its major downfalls.

Figure 2.6. Roll of AFRP Sheets [14]

Basalt FRP

Similar to other FRP's, basalt FRP (BFRP) can be used as external or internal reinforcement and lies between glass and carbon in terms of its stiffness and strength [18]. Although BFRP is not as commonly researched as CFRP and GFRP, it does offer some advantages when utilizing it. When compared to other types of FRP, BFRP is cost effective, has a relatively simplistic method of manufacturing, and has strong resistance to high temperatures [18].

Figure 2.7. BFRP Reinforcing Bars [19]

Hybrid FRP

When dealing with FRP, a common technique is to manufacture a hybrid FRP material. Unlike a composite material such as CFRP or GFRP, which is manufactured solely from that type of fibre, a hybrid consists of more than one type of material. This is done in order to capture the benefits of each separate material, but in a fashion that compliments one another. An example of this is a steel-FRP composite bar (SFCB), which utilizes the high strength of steel while mitigating the damaging effects of corrosion through the addition of

FRP. In most instances, the FRP outer shell is created from an aramid or vinylon fibre [20]. Figure 2.8 provides the general layout of a SFCB.

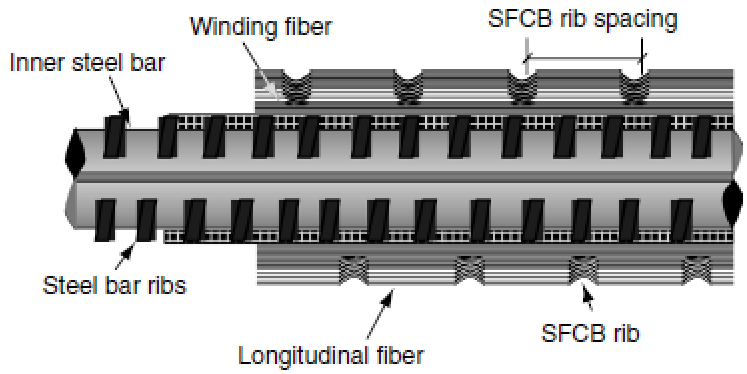

Figure 2.8. Steel-FRP Composite Bar [20]

2.3.1 Fibres

Fibres, as a 3D composite material, can be manufactured in many ways. Depending on the desired material properties, the manufacturing process can be performed through weaving, braiding, knitting, and stitching [21].

Weaving

Weaving is the most popular manufacturing technique for fibres and is the most common practice within the composite industry [21]. This method is typically used when producing single layer fabrics, such as with carbon and glass. In a traditional, two-dimensional (2D) sense, weaving consists of interlacing two sets of fibres to create an interlocking pattern, as demonstrated below.

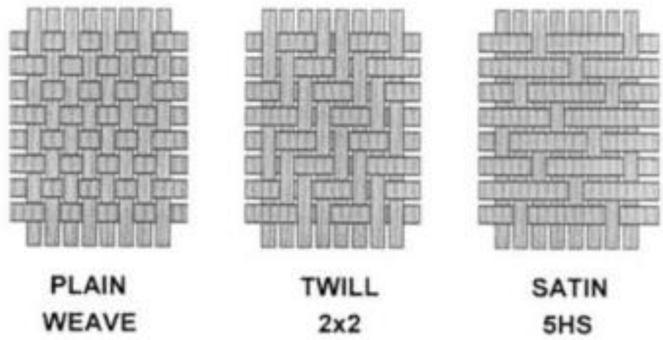

Figure 2.9. Two-Dimensional Weaving Patterns [21]

When producing a fibre composite material sheet, the weaving pattern is more complex as it is dealing with a 3D weave rather than 2D. The general procedure behind it, however, is essentially the same as the 2D method. The weaving technique is typically used in manufacturing large volumes and widely dimensioned pieces.

Braiding

Braiding is the second most common process of manufacturing FRP's. Much like weaving, the braiding technique involves interlocking several strands of fibre. Tong et al. [21] describes its usefulness when developing narrow width or tubular pieces of fabric, quite opposite to typical woven FRP materials.

Knitting & Stitching

Knitting and stitching are the least practiced and most outdated methods of FRP manufacturing. Further information of these two techniques can be further research in [21].

2.3.2 Resins

When using an FRP material, one of the most important components is the resin. Hojo et al. [22] explain that the performance of the FRP is directly linked to the performance of the resin matrix. The resin, which is applied directly to the FRP material, is essentially the glue that holds the fibres together and distributes the load between them. Furthermore, it also acts as the adhesive between the FRP material and the substrate [23]. Therefore, a properly adhered FRP material is key in ensuring its capacity is being fully utilized.

When applying the FRP and resin, the two commonly used methods of application include the pultrusion method and the lay-up method. The first of the two is a prefabrication method used to create specific shapes, such as beams, plates, sheets, and rods. The fabrication of the FRP part occurs at an off-site factory, where the resin saturated fibres are heated and moulded into a shape through a controlled process. While this may yield very consistent and uniform results with minimal defects, it can also cause significant issues during its application. Due to its prefabrication, the FRP composite material has minimal flexibility and cannot always adapt to potential unpredicted configurations and dimensions encountered during its application that were not originally accounted for [23]. This can be a common occurrence in the construction industry as site specifics often change as progress develops.

The second application technique, commonly known as a wet layup, is an in-situ application on the substrate itself [23]. Typically used when installing FRP sheet, the wet layup method provides extreme flexibility of the FRP material, allowing for the geometry of the structure to be rehabilitated to be closely fitted [24]. As explained by Sciolti et al. [24], the bond configuration between the FRP material and the substrate typically consists of a resin with similar properties to the composite, resulting in a stronger, interlayer bond. There are, however, some concerns when dealing with a wet layup procedure, as there is a lot less control over the final product when compared to the pultrusion method. Since a wet layup is not machine controlled, its application sequence is crucial in yielding proper results. Therefore, the quality of the final product will typically hinder on the application technique and procedure.

In terms of types of resins, there are two main different types: thermosets and thermoplastics. The former of the types, thermosets, are the most common. This is due to the fact that they cannot be altered from reheating, therefore making it irreversibly hardened upon application. Within the group of thermosetting resins, epoxy resins are typically used in structural applications due to their relatively low cost, flexibility, and high strength [24]. Thermoplastics, the less common type, is a viscous resin that is transforms into a liquid in heat, hardening once cooled [25]. Therefore, unlike thermosets, thermoplastic resin is reversible once heat is applied. Although this can be ideal in certain scenarios, there are many situations where having a material liquify once exposed to heat that make it not ideal.

2.4 Externally Bonded FRP Sheets

In the industry, the use of FRP composite materials are becoming more common through the use of pre-cured systems, wet layup systems, or prepeg systems [26]. The first method, pre-cured systems, is the application of FRP as internal reinforcement such as a strip or bar. As discussed in Section 2.3, there are a variety of types and applications of FRP. GFRP, for example, was described as typically being incorporated as an internal reinforcing bar. Although not always the case, FRP bars are typically used as internal reinforcement when they are solely representing the entire reinforcement of the member, not acting as a supplementary aid to the existing reinforcement. When FRP is used as a means to strengthen and rehabilitate an existing member, it is most commonly done with an externally placed sheet or plate. This is the second method of FRP application, known as external reinforcement.

Retrofitting existing concrete structures with externally bonded FRP sheets is becoming a widespread strengthening and rehabilitation method in the construction industry and is beginning to gain a lot of recognition in design codes and standards [6], [3]. Aside from the relatively easy application of the external bonding method, the main benefit derives from the fact that the shear and normal stress are transferred by the resin layer [27]. Although FRP wrapping can be done in a number of different ways, ACI Committee 440 [11] suggests three types of wrapping to increase shear strength, as shown in Figure 2.10.

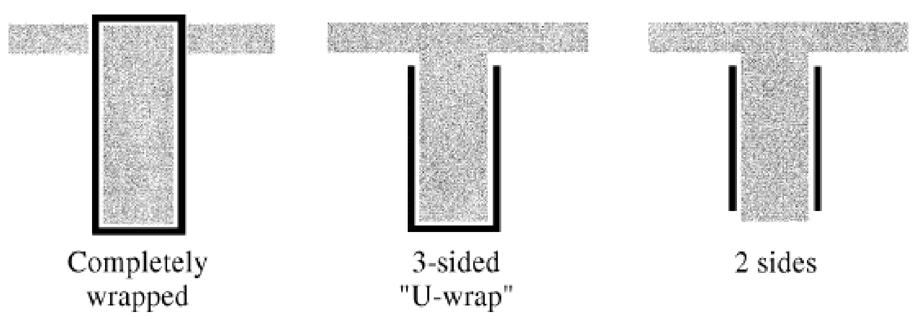

Figure 2.10. FRP Wrapping Schemes [11]

The bond between the external FRP sheet and the concrete has the ability to properly transfer the load from the degrading concrete member and distributed it amongst the FRP member and its fibres. This allows the FRP material to make proper use of its strengthening capabilities. Furthermore, using FRP sheets as external reinforcement presents an attractive solution when compared to more traditional methods such as steel plates as steel is much more labor and equipment intensive [28].

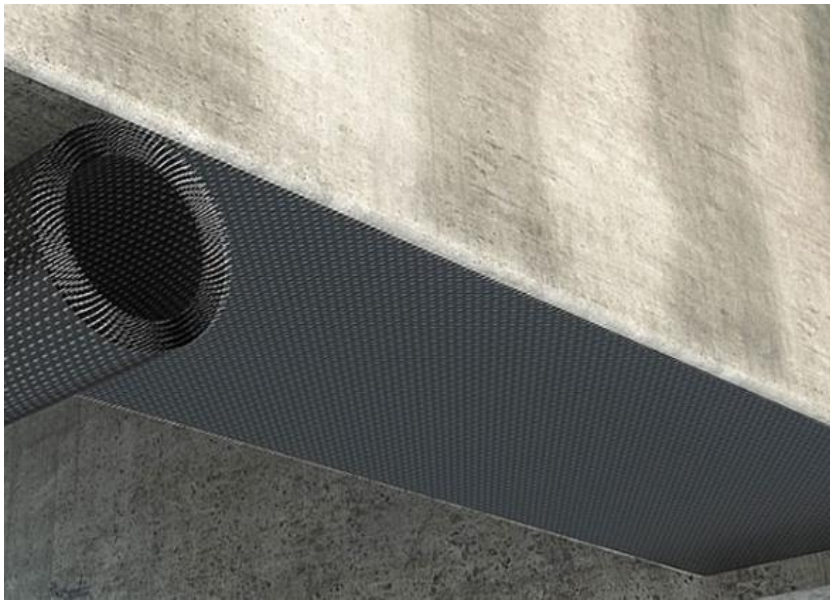

Figure 2.11. CFRP Sheet Externally Bonded to Beam [29]

There are also similar application techniques to the external bonding of a sheet such as the near surface mounted (NSM) application. This application is conducted by inserting an FRP sheet or bar into slit saw cuts, which results in additional bonding area and confinement by the concrete [26]. An example of this can be seen in Figure 2.12 and Figure 2.13.

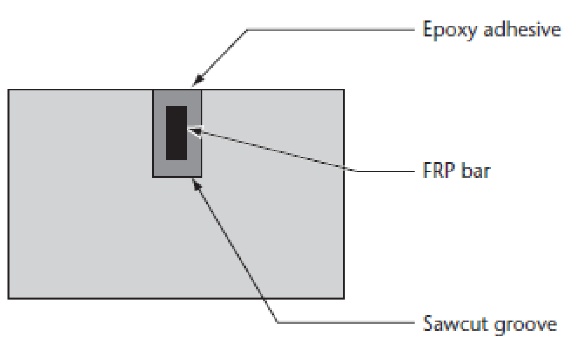

Figure 2.12. Near Surface Mounted CFRP [30]

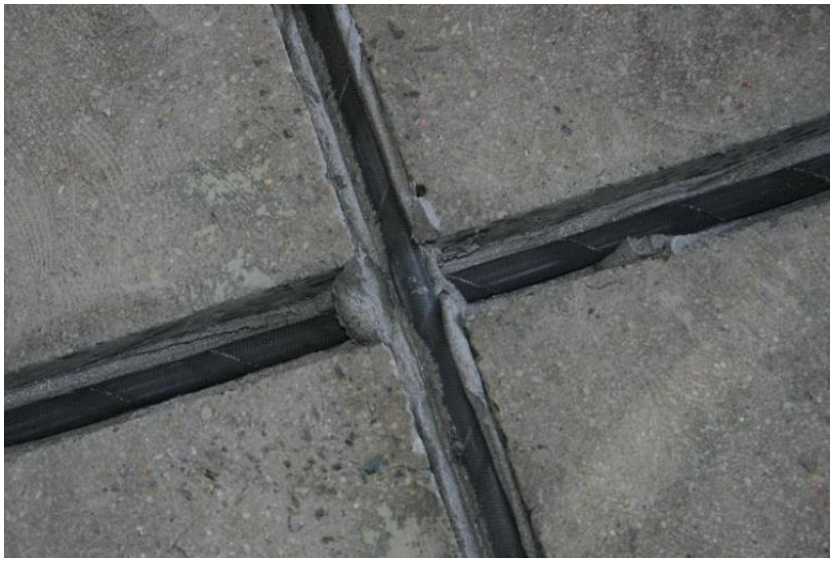

Figure 2.13. Field Application of NSM CFRP [31]

2.5 Experimental Studies

2.5.1 Testing Methods

There are a variety of different testing procedures when conducting experimental studies with FRP. As expected, the selected testing methodology is dependent on the desired goal of the results. Therefore, conducting the same study with different test setups can lead to quite a change in results. The more common test methods when dealing with FRP externally bonded to concrete include: direction tension, three- or four-point bending, single or double lap push, single or double lap pull, and peel tests [32]. Figure 2.14 demonstrates the basic overview of each of the tests previously listed.

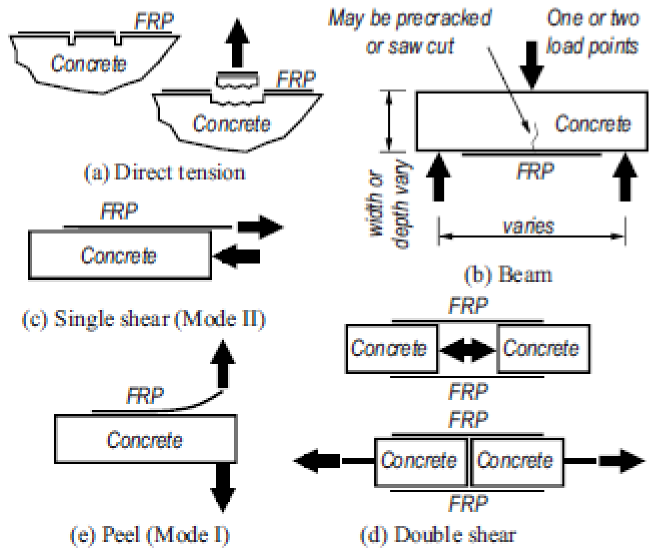

Figure 2.14. FRP-to-Concrete Test Methods [32]

A study conducted by Gartner et al. [32] investigates which testing method is appropriate for measuring the durability of the bond strength of a CFRP sheet externally bonded to concrete. After testing a number of different beams with varying size and material properties (i.e concrete strength), it was concluded that the three-point bending was the most suitable test method.

Nguyen et al. [33] conducted an experimental study that investigates the different failure modes of CFRP bonded to concrete. This test conducted four-point bending on several different specimens, determining the three observed failure modes of ripping of the concrete (tension failure), premature shear failure, and hybrid [33]. Three and four-point bending are common test methods mainly due to their simplistic setup and ability to conduct the tests using a universal testing machine [32].

According to Hosseini et al. [34], conducting a single shear pull test was most appropriate when investigating the effective bond length of FRP-to-concrete adhesively bonded joints.

This was done in order to eliminate stress concentrations at the CFRP end under loading [34].

Each test method has their own unique capabilities, making them all useful in some form or another. The specifics the study is investigating is, for the most part, the main driving force behind the reasoning to use a specific test over others. Depending on the study, certain design standard and codes may have recommended testing methods as well. The Canadian Standards Association (CSA) S806-12, for example, has the pull test as their recommended test setup when designing and constructing with FRP.

2.5.2 Bond & Development Length

According to Nguyen et al. [33], the development length of an FRP material bonded to another member is defined as the distance at which full composite action occurs. Also known as the effective bond length or the effective transfer length, the development length can be summarized as the bond length in which maximum capacity is obtained, and any lengthening of the bond beyond that point will not result in any capacity increases [35]. The difficulty surrounding development length comes from the ability to accurately predict it. While obtaining bond development length from experimental studies is straightforward, deriving an appropriate theoretical formula can be difficult. The ACI Committee 440 for example, specify Chen and Teng's model [36] in determining the appropriate development length of externally bonded FRP [11]. This equation can be found below, which incorporates FRP's tensile modulus of elasticity, the thickness of one ply of the FRP material, and the compressive strength of concrete.

$$l_{df} = \sqrt{nE_f t_f / \sqrt{f_c'}} \tag{1}$$

Although much research work has been conducted on the bond and development length of FRP externally bonded to concrete, only a select few of the numerous models proposed in research have been adopted by design standards and codes [34].

The study conducted by Nguyen et al. [33] investigates the strengthening of concrete beams through CFRP plates and concludes that, while different bond lengths of CFRP were tested, the development length remained nearly constant. A separate study performed by Hosseini et al. [34] comparing different theoretical bond development length models established similar conclusions. While all three models had varying development lengths from one another, they remained consistent with their own respective models regardless of an increase in bond length. This is demonstrated in the table below, where *Lf* and *Le* represent the FRP bond length and effective (or development) bond length, respectively.

Table 2.2. Effective Bond Lengths of Theoretical Models [34]

Test specimen	f_c (MPa)	L_f (mm)	L_e (mm)		
			fib Bulletin 14 [27]	Chen and Teng [3]	Seracino et al. [24]
EBR-20-1(2)	36.8	20	69.0	71.7	42.2
EBR-35-1(2)	36.8	35	69.0	71.7	42.2
EBR-50-1(2)	36.8	50	69.0	71.7	42.2
EBR-75-1(2)	36.5	75	69.1	71.8	42.3
EBR-100-1(2)	36.5	100	69.1	71.8	42.3
EBR-125-1(2)	39.1	125	67.9	70.6	41.5
EBR-150-1(2)	39.1	150	67.9	70.6	41.5
EBR-175-1(2)	41.1	175	67.1	69.7	41.0
EBR-200-1(2)	41.1	200	67.1	69.7	41.0
EBR-225-1(2)	40.6	225	67.3	70.0	41.1
EBR-250-1(2)	40.6	250	67.3	70.0	41.1

2.5.3 Failure Modes

From previous research conducted on CFRP sheets externally bonded to reinforced concrete, there are several different failure modes that can occur. Typical failure modes include debonding failure, concrete cover separation, concrete crushing/ripping, shear failure, and FRP rupture [33], [37], [38].

A large majority of the previous research and experimental studies, however, lead to reoccurring conclusions that debonding is the most common mode of failure. When debonding occurs, it will be the cause of the resin, FRP, or the concrete. When this failure mode occurs due to the resin or FRP, either the capacity of the material is not sufficient under its current loading condition or the material was applied in a poor or incorrect manner. When debonding occurs due to the concrete, it is most commonly the result of the concrete failing in tension. As previously observed in the results of [35], debonding occurred by shearing of the concrete below the bonded surface due to tensile failure. Therefore, the cause it associated with the concrete itself and not the bond.

This presents several significantly negative impacts that debonding has on FRP material in general. Firstly, a premature debonding an FRP sheet from a concrete member indicates that the full tensile strength of the FRP composite material is not fully utilize [39]. Therefore, it can be concluded that the bond between the two members can be a critical yet limiting factor, further solidifying the fact that the performance of the FRP material is often hindered by the bond [3]. Therefore, it "plays a critical role in ensuring the effectiveness of this strengthening method" [3].

The second main issues with debonding failure is its suddenness. CFRP has a very brittle failure mode that can be difficult to predict prior to it occurring. Given that it is typically structures retrofitted with CFRP, safety is a major concern as failure of the material can be catastrophic. Research work conducted by Obaidat et al. [40] sheds light on their concerns with studies of other researchers, as they indicate that "very few studies have focused on structural members strengthened [with CFRP] after preloading" despite its growing popularity. Therefore, a better understanding of debonding failure along with the other common types of failures modes encountered with FRP material.

2.6 Numerical Studies

Although CFRP reinforcement is widely known and gaining popularity at an increasing rate, there is limited amount of numerical studies conducted on it, such as finite element modeling (FEM).

2.6.1 Finite Element Modelling of FRP Sheets Externally Bonded to Reinforced Concrete

Using a finite element analysis software to conduct modelling can provide many benefits if done so correctly. While the traditional experimental studies involving testing does provide many benefits and further developments, there are many aspects of FRP materials that cannot be fully understood using exclusively testing [5]. As such, many researchers are beginning to utilize finite element modelling and its capabilities to pursue studies on a different scale.

Barbato [6] carried out an numerical study regarding a two-dimensional finite element model capable of accurately predicting the capacity of a reinforced concrete beam externally strengthened with FRP strips and plates. As discussed in Section 2.5, the common modes of failure encountered during each simulation included concrete crushing, rupturing of the FRP material, and debonding of the FRP-to-concrete interface [6]. Al-Zubaidy et al. [41] investigated the finite element model of CFRP material used as a double strap joint. By comparing to previous experimental results, researchers were able to validate their effective bond length determined by the analysis. Furthermore, it was determined that the two reoccurring failures modes included debonding between the material as well as CFRP delamination [41].

2.6.2 Concrete Crack Propagation in Finite Element Analysis

The difficulty of modelling CFRP sheets externally bonded to reinforced concrete stems from the ability to accurately model concrete. Unlike steel, it is often challenging to properly model concrete due to its unpredictability when reaching failure. Therefore, having a thorough understanding of the crack propagation in concrete will lead to much more suitable results.

Chen et al [42] conducted research on reinforced concrete beams with shear-strengthened with FRP and discussed the challenging nature of accurately modelling concrete shear cracks, which, in their opinion, is a direct link to the lack of numerical studies surrounding FRP. To further add, the debonding failure between FRP and concrete can often be a result to localized cracking of the concrete, further solidifying the difficulties in modelling concrete [42]. When dealing with crack propagation and concrete fracture in a finite element setting, there are two dominant methods in modelling concrete cracking: the discrete crack model and the smeared crack model [42]. Discrete crack modelling simulates an initial geometrical crack with it propagating into dominant cracks. The smeared crack model, however, is a constitution of numerous small cracks that form into larger dominant cracks as the model analysis progresses [43]. A simplistic representation of the initiation of a discrete crack model can be found in Figure 2.15.

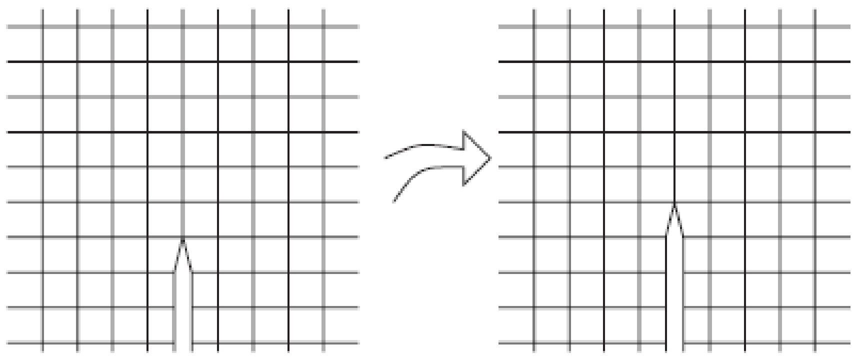

Figure 2.15. Early Stage of Discrete Crack Model [43]

The two different cracking models each have their respective fields. As explain by de Borst et al. [43], discrete crack models are mainly used to model a small number of dominant cracks while the smeared crack models are used to model smaller cracks and simulate cracking patterns.

2.6.3 Concrete Damage Plasticity

Concrete damage plasticity (CDP) is another common technique used when modelling the behaviour of concrete. In the finite element software ABAQUS, concrete damage plasticity characterizes the tensile and compressive response of concrete by Figure 2.16.

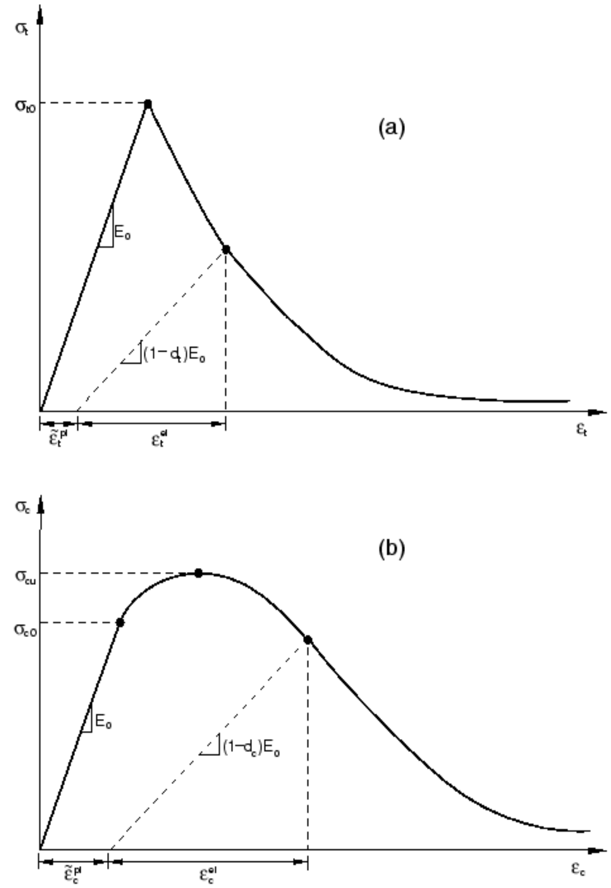

Figure 2.16. Tensile (a) and Compressive (b) Response of Axially Loaded Concrete Using CDP [44]

The benefit of a CDP model is its allowance to capture the behaviour of concrete through elastic damage models and elastic plastic laws [45]. Therefore, compression and tension damage parameters can be introduced to the concrete model, which results in a more accurately defined material. Ultimately, it considers crushing due to compression and cracking due to tension as failure modes [46]. The CDP modelling inputs, however, can often be difficult to determine if there is not a thorough understanding of the material and its parameters.

2.7 Literature Review Conclusion

From the research done in this section, it is evident that FRP is becoming a popular rehabilitation method in the construction industry. There are many different types of FRP such as carbon, glass, aramid, and basalt. It has a wide variety of uses and applications, such as an internal reinforcing FRP bar or an externally bonded FRP sheet. Externally bonded FRP sheets are typically comprised of carbon and are commonly applied to deteriorating reinforced concrete.

Based on various experimental testing and numerical models, it can be concluded that the most common failure for FRP sheets externally bonded to reinforced concrete is debonding. Wen this failure mode, the full capacity of the FRP material is not fully utilized. Therefore, a better understand of the bond behaviour at the FRP-concrete interface is needed. When investigating bond behaviour, a common parameter to consider is the development length, or effective bond length, of the FRP material bonded to the concrete. From previous studies, many researchers have found that development length tends to remain mostly the same regardless of an increase in the FRP's bond length to the concrete. Although there are many different methods in determining the development length, this is a constant theme throughout.

Numerical modelling with finite element software provides an excellent tool to examine the bond behaviour of FRP sheets bonded to concrete. Finite element software provides users with a variety of different construction methods to model this system. In general, the FRP-concrete interface can be modelled as a perfect bond, by defining a friction interaction between the two materials, or as a cohesive layer between the FRP and concrete. Numerical modelling of FRP materials is still a relatively new field with limited research. There are numerous input parameters and functions when constructing a finite element model, therefore it can be difficult to provide an accurate representation of the model without solid experimental testing. A thorough understanding of not only the software being used but also the materials being modelled is a necessity to provide a well developed and accurate model.

3.0 EXPERIMENTAL STUDY

3.1 General

The precedent study to this project was an experimental investigation conducted as a Master's thesis by E. Atunbi [35] at the University of New Brunswick. The experimental study, as aforementioned, involves the study of bond behaviour of CFRP-to-concrete interface. More specifically, it investigates the effects of bond length and stress on the CFRP-to-concrete system under static loads. This experimental study, taken place over the course of several months, incorporated twelve different specimens subjected to a double lap shear pull off test. In order to obtain a better understanding of the reasoning behind the finite element model, a brief explanation of the experimental study will be outlined in the following sections.

3.2 Specimens

The test specimens of the experimental study used four materials: concrete, steel rebar reinforcement, CFRP sheets, and resin (epoxy). Each specimen was constructed in similar fashion, consisting of two reinforced concrete prisms butted end to end with a 3 mm gap between the two. The prisms had a single strip of CFRP sheet attached on both the top and bottom face. Figure 3.1provides a general layout of the test specimen.

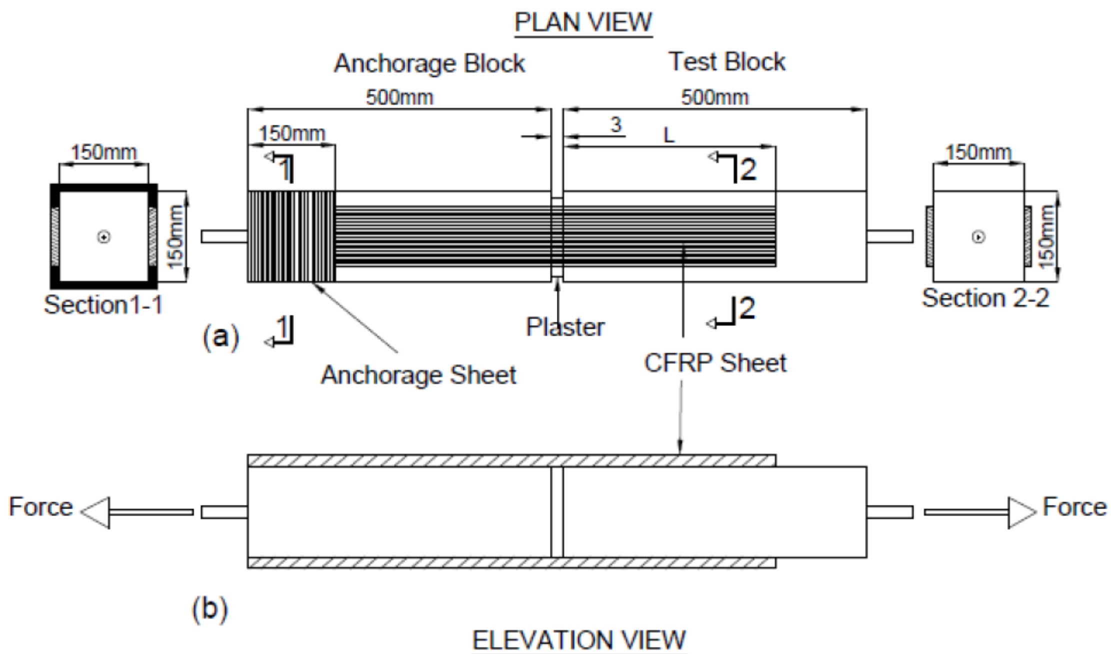

Figure 3.1. Layout of Experimental Test Specimen [35]

The difference in the test specimens, however, comes from the bond length of the CFRP sheet. For comparative purposes, three different bond lengths were used: 160 mm, 240 mm, and 350 mm. As noted previously, twelve specimens in total were tested, which were split evenly amongst the three varying bond lengths.

A more thorough breakdown of each material used within the specimen is explained below.

3.2.1 Reinforced Concrete Prisms

The concrete prisms used for the test specimens were cast using ready mix concrete in dimensioned plywood forms. The prisms had a cross sectional dimension of 150 mm by 150 mm with an overall length of 500 mm. Located in the middle of each prism was a single 20M reinforcing steel bar, which was casted with one end slightly protruding for testing purposes. Proper curing times were ensued for each specimen, which yielded a 28-day average compressive strength of 34.3 MPa.

3.2.2 CFRP Sheets & Epoxy

For the construction of the test specimens, commercially manufactured CFRP sheets and epoxy from the industry were purchased and used. MasterBrace FIB 300/50 CFS was selected as the CFRP sheet, described as a unidirectional high strength carbon fibre [47]. As indicated on the technical specification sheet, the CFRP has a nominal dry thickness of 0.165 mm and width of 500 mm, and is used on concrete, masonry, timber, and steel substrates. The epoxy used in this testing consists of three different components, as per MasterBrace's recommendation on the application of CFRP sheets. The bonding system includes a primer, MasterBrace P 3500, a putty, MasterBrace F 2000, and a saturant, MasterBrace SAT 4500. As indicated above, the CFRP sheets were adhered to the concrete prisms at three different bond lengths of 160 mm, 240 mm, and 350 mm.

3.2.3 Coupon Testing

To obtain a better understanding of the properties of the CFRP and epoxy, coupon tests were conducted. The coupons, subjected to tensile testing in correspondence to Annex F of CSA S806-12, were comprised of a single CFRP sheet with a specified gauge length of 340 mm and width of 38 mm, coated with the epoxy, or saturant. A total of five coupons with identical properties were created and tested using an Instron testing machine with a capacity of 250 kN. The following table provides a summary of the average properties calculated based on the tensile testing of five separate coupons.

Table 3.1. Mean Results of CFRP Coupon Tests

Specimen	Ultimate Load (kN)	Ultimate Strain (%)	Tensile Strength (MPa)	Modulus of Elasticity (GPa)
Coupon 1 - 5	24.4	0.019	641.6	37.84

For simplicity sake, a thickness of 1 mm was assumed for the combined CFRP and epoxy coupon, which was used in calculating the results.

3.3 Testing

The double lap shear pull off tests were performed on the twelve different specimens "using a universal testing machine in the Structures Laboratory of the University of New Brunswick" [35]. The steel reinforcing rebar of each specimen was casted in a manner that had each end slightly protruding from the centre of the concrete member. This was done in order to allow for the testing machine to properly grip the specimen. Each specimen was subjected to static loading with a continual displacement load rate of 0.5 mm per minute until reaching failure. Each of the twelve specimens, with varying specified bond lengths, were subjected to the double lap shear test, as outlined in Figure 3.2.

Figure 3.2. CFRP-Concrete Specimen Loaded on Universal Testing Machine [35]

In order to accurately measure the results of each specimen, a digital image correlation (DIC) technique was used. The DIC, as described by Dantec Dynamics [48], “is a 3D, full-field, non-contact optical technique to measure contour, deformation, vibration and strain on almost any material”. For the experimental investigation of the CFRP-concrete interface, the DIC allowed proper measurements and monitoring of the specimen’s response throughout its progression from the initial displacement to the point of failure. This was accomplished by using digital cameras to capture the test specimens and their progression of displacement through the loading cycle. The cameras are set to capture images at a given time interval, which are compared to the initial, undeformed specimen. During the testing, the load values experienced by the specimen were recorded every 0.1 seconds while the strain values were only recorded every 0.4 seconds. Upon completion of the test, the data was analyzed using VIC-3D, a powerful software analysis tool used for processing the images resulting from the DIC technique [49]. An example output of the processed data can be found below in Figure 3.3.

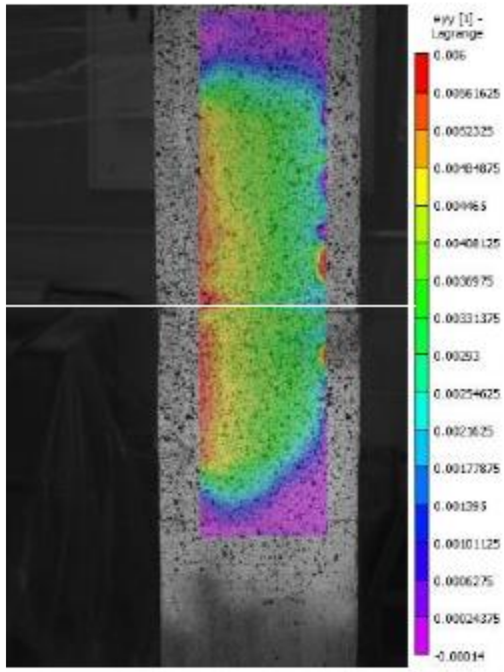

Figure 3.3. Example of Distribution of Longitudinal Strains using VIC-3D [35]

3.4 Results

The three different bond lengths that were subjected to static loading are 160 mm, 240 mm, and 350 mm. A total of twelve specimens were testing in the laboratory, therefore there were four specimens per bond length. According to Atunbi [35], the reoccurring failure modes of the test specimens was tensile failure of the concrete. Although the CFRP sheets were debonded from the specimen upon failure, it was noted that this was not the governing failure mode as a substantial amount of concrete remained bonded to the sheet when it came apart from the specimen. A brief summary of the failure loads experienced by the specimens can be found in the table below.

Table 3.2. Average Failure Loads of Test Specimens

Specimen	Bond Length (mm)	Failure Load (N)	
		Average	Variance
S1 – S4	160	38 667	4.7
S5 – S8	240	43 382	20.9
S9 – S12	350	40 111	21.9

From inspection of Table 3.2, it can be determined that the increase in bond length did not cause any significant increase in the specimen's capacity. A similar outcome can be concluded from the longitudinal strain and effective bond length measured during testing.

Table 3.3. Average Longitudinal Strain & Effective Bond Length of Test Specimens

Specimen	Bond Length (mm)	Longitudinal Strain (%)		Effective Bond Length (mm)	
		Average	Variance	Average	Variance
S1 – S4	160	0.54	0.0062	50.0	66.7
S5 – S8	240	0.64	0.0029	55.0	100
S9 – S12	350	0.57	0.0023	57.5	25.0

Although the majority of the specimens have failed through debonding of the CFRP to the reinforced concrete prisms, the results indicate that the increased bond length does not increase the specimen's failure load. It should be noted that the failure load is larger for the specimens when increasing from 160 mm bond length to 240 mm, but reduces again when increase the bond length from 240 mm to 350 mm. Atunbi [35] suggests that this should be further investigated, as a similar trend can be seen in the longitudinal strain of the test specimens.

4.0 NUMERICAL MODELLING

4.1 General

In order to analyze the behaviour of system consisting of reinforced concrete members externally reinforced by CFRP sheets, several different methods are available. Chapter 3 of this project, Experimental Study, provides a prime example of how such data can be collected through experimental testing. Although it can prove to be a very robust, reliable, and efficient manner in obtaining results, it does have its shortcomings. The time required in order to conduct appropriate tests, for example, can oftentimes be quite significant. The test specimens used in the double lap shear pull off tests referenced above required several months to reach testing capabilities. As described by E. Atunbi [35], the CFRP sheets were placed on the concrete specimens 51 days after they were cast, while the testing occurred 87 days after the sheet were installed. Furthermore, the economical aspect involved in experimental testing can often be cumbersome, with expenses progressively climbing through ongoing specimen fabrication and testing throughout the entire process.

Numerical analysis is another means of analyzing problems. Traditionally, using numerical methods was not always the favourable approach of approximation when dealing with relatively simple problems due to its complexity. It is, however, becoming a more widely used tool due to major advancements in computer programming and software development. Examples of the varying numerical methods include [50]:

- Finite Element Method (FEM);
- Boundary Element Method (BEM);

- Finite Difference Method (FDV);
- Finite Volume Method (FVM), and;
- Meshless Method (MM).

Finite element method, one of the more common types of numerical methods, is typically exercised in engineering related applications. Introduced by Clough, FEM is described as a “standard methodology applicable to discrete systems” which is used as a means of determining approximate results of simplified models [51]. The result of a simplified model is achieved through the transformation of complex systems into smaller, more manageable elements, which are essentially subdivisions of the overall model. When in application, FEM is often paired with a process known finite element analysis (FEA). FEA can be described as the process of producing an accurate approximation of the reaction of a product to real world scenario through the use of software simulation [52].

In order to construct an adequate finite element model with the capability of reproducing accurate results, acceptable properties and parameters must be correctly specified. Due to this, FEA and its potential level of subjectivity is one of its main downfalls. Although this can be a relatively small obstacle to overcome, it still requires careful planning, consideration, and a thorough understanding to avoid all together. This can be accomplished by ensuring all inputs, such as material properties, boundary conditions, and model constraints are appropriate representations of the desired scenario. Although a lot of the inputs incorporated in FEA can be adequately obtained through literature research, past analyses, textbooks, and standards, some of the parameters require more extensive research through additional experimental studies and testing.

Finite element analysis can also be perceived in a negative manner due to the fact that it is only an approximation. Referencing back to the issue of FEA and its subjectivity, obtaining the approximate solution of a model can vary. Furthermore, models constructed using FEA will oftentimes be idealized scenarios resulting in unrealistic results. Therefore, it is of good practice when dealing with FEA models to have a method to measure the results, indicating whether or not the analysis was an accurate representation. Oftentimes this is accomplished through the comparison of experimental results, previously constructed FEA models, and even rudimentary hand calculations. There are also some instances when the level of accuracy cannot be appropriately measure, which requires a strong working knowledge of the model construction and its parameters.

Finite element analysis modelling can be a very powerful tool when used properly. FEA has a very high ceiling when it comes to its ability dealing with complex structures and scenarios by creating smaller, more manageable systems. With the advancement in technology as well, finite element software is reaching new heights with its impressive computing time, problem solving and algorithm capabilities, and results. Performing experimental studies in a laboratory can be very limiting as the study is often limited to the available materials and testing equipment on site. FEA simulation, however, is providing researchers with the opportunity to conduct the necessary further and more detailed investigations of their studies, which is only limited to the software itself.

4.2 Software

There are many different tools on the market capable of conducting numerical analysis. As expected, each of the tools, although similar from a high-level view, can be vastly different when comparing specifics. One of the most common tools used for numerical analysis and simulation is finite element analysis software. There are several different FEA software packages that are popular in the industry, which are briefly described below.

- ABAQUS: Powerful simulation tool capable of computing solutions for basic to complex engineering problems. The uses include “dynamic vibration, multibody systems, impact/crash, nonlinear statics, and thermal coupling” [53].
- ANSYS: An engineering simulation product used in predicting how designs will react in real-life scenarios [54]. Similar to ABAQUS, ANSYS measures mechanical and electromagnetic properties, as well as fluid dynamics.
- LS-DYNA: A non-linear, dynamic finite element analysis that uses explicit time integration to conduct complex simulation [55]. LS-DYNA is operated through command lines and considered one of the more flexible FEA softwares.
- Nastran – Originally developed for NASA, Nastran is a finite element analysis tool used to perform “static, dynamics, and thermal analysis across the linear and nonlinear domains” [56]. It is also highly recognized as an embedded fatigue and vibration fatigue simulation tool.
- HyperMesh: A preprocessing finite element modeling software capable of importing CAD and other solver interfaces [57]. HyperMesh is primarily considered a meshing software.

Although the list above is a very small subset of available finite element software, it is evident that the majority of them have similar capabilities. The basic capabilities and outputs sought after in a FEA software would include the following [52]:

- Stress;
- Strain;
- Deformation;
- Displacement;
- Fatigue;
- Heat transfer; and,
- Fluid dynamics.

The small differences that can be found between each software, however, is the deciding factor. Whether the user is looking for the ability to properly model vibration fatigue and cohesion elements, or the model requires an advanced meshing program, certain software will cater to specific needs. Therefore, while all of the software listed above along with many more prove to be a strong choice in FEA modelling both in the academic and industry world, the preference ultimately depends on the user and their needs.

4.2.1 ABAQUS

In order to properly model CFRP sheets externally bonded to reinforced concrete subject to a double lap shear test, two similar types of software were investigated: ABAQUS and ANSYS. ABAQUS was ultimately selected as the FEA software of choice for a number of reasons. The main reason for using ABAQUS is due to its ability to model cohesive elements. Furthermore, the number of available constraint options when modelling with ABAQUS allows for a more proper replication of a FRP sheet bonded to another member. Finally, given the University’s available licensing with the software, ABAQUS was the optimal choice.

4.3 Assumptions

To successfully conduct the numerical modelling, several assumptions were made. These assumptions, whether regarding the numerical or previously conducted experimental portion of the reason, are in place to provide clarity, consistency, and simplicity where needed. The assumptions that have been made include the following:

- ABAQUS, as a finite element analysis software, is adequate to construct a model of replicating CFRP sheets externally bonded to reinforced concrete;
- The homogeneity of the materials is in place to represent the actual materials that are being used;
- The bond between CFRP and reinforced concrete is perfect;
    - This assumption will be discussed in greater detail in Chapter 5.
- The CFRP sheet saturated with the epoxy has a thickness of 1 mm;
- The displacement between the CFRP sheet and the concrete at the unloaded, free end, is negligible;
- There is no displacement between the steel reinforcement within the concrete and the concrete itself; and,
- The experimental test specimen is fully symmetric about its axis and can be modelled as such.

5.0 FINITE ELEMENT MODEL CONSTRUCTION

5.1 Material Properties

When using a finite element analysis software such as ABAQUS, the crucial factors in developing an accurate model comes from the materials used and their respective properties. When past experimental results are not readily available, or parameters are unknown, certain properties will have to be derived from educated assumptions, be it through literature search or background knowledge regarding the subject. This presents a certain level of difficulty when working with ABAQUS and other similar FEA software, as the often complex and vast material properties will be the deciding factor in determining the model's level of accuracy.

The following sections will contain a summary of each of the materials used and their respective properties inputted in the finite element model. This project incorporates four different materials into the construction of the CFRP bonded to concrete model, which includes: concrete, steel, CFRP, and epoxy.

5.1.1 Concrete

The initial model consisted of two concrete prisms to represent the ready-mix concrete used for the experimental test specimens. The concrete material was divided into two different material behaviours: elasticity and plasticity.

Elasticity

For the elastic behaviour, several different types can be selected such as: linear elasticity, hyperelasticity, low density foam elasticity, porous elasticity, viscoelasticity, etc. The elastic behaviour of concrete is only linear for a short period of time and becomes a non-linear, plastic behaviour once reaching its yield point. This is demonstrated in Figure 5.1 outlining the typical stress-strain response of concrete, including prestressed and normal reinforced concrete [58].

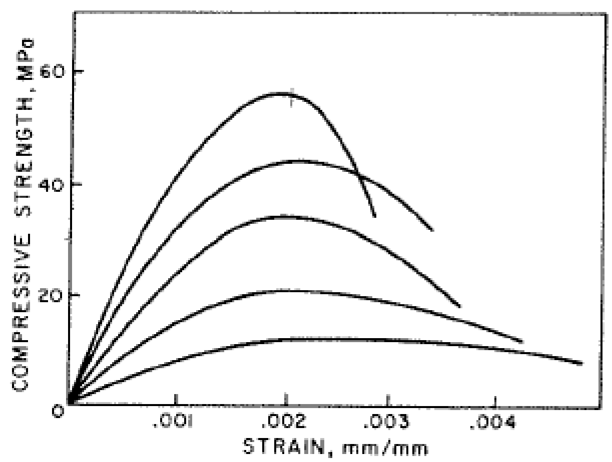

Figure 5.1. Typical Stress-Strain Response of Concrete [58]

Therefore, linear elasticity behaviour is used to represent concrete as it is the most basic and relevant type to use in ABAQUS. In order to determine the value of Young's modulus, E_c, the compressive strength of the concrete was incorporated into the follow equation.

$$E_c = 4500\sqrt{f_c'} \tag{2}$$

It should be noted that the compressive strength of 34.3 MPa of the concrete is the result of the average 28-day compressive strength measured from the concrete test cylinders casted during the experimental study.

From previous literature reviews as well as reinforced concrete standards and textbooks, a Poisson's ratio of 0.2 was selected to best represent the concrete material. As this is a homogeneous, isotropic material, the Poisson's ratio, ν, of the concrete is directly correlated to the shear modulus, G, and the Young's modulus, E, as demonstrated in the equation below. This is also known as one of the Lamé parameters [59].

$$\nu = \frac{E}{2G} - 1 \tag{3}$$

The shear modulus of concrete is not a direct input into ABAQUS but rather calculated by the software itself using the Young's modulus and Poisson's ratio values.

In order to determine the tensile behaviour of concrete, the three main methods of measure were investigated: direction tension, splitting tension, and modulus of rupture [58], [60]. The first method, as outlined in Figure 5.2, is the direct tension.

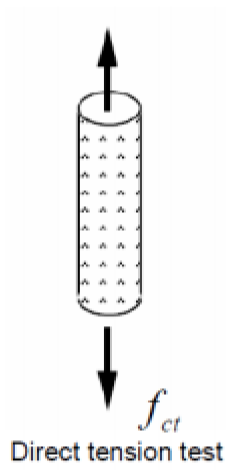

Figure 5.2. Tensile Strength – Direct Tension [60]

As the name implies, the method is used when testing concrete solely in tension. Although it is considered as the most direct way to measure tensile strength of concrete, uniaxial tensile testing is not as commonly used as the other two. This can be attributed to the difficulties in properly gripping the concrete specimen to conduct uniaxial tension. The following equation represents the tensile strength of concrete under direct tension.

$$f_t = 0.33\lambda\sqrt{f_c'} \tag{4}$$

The second form of tensile strength measurement is called the splitting tension test. This involves splitting a cylindrical test specimen down its center, as shown in Figure 5.3.

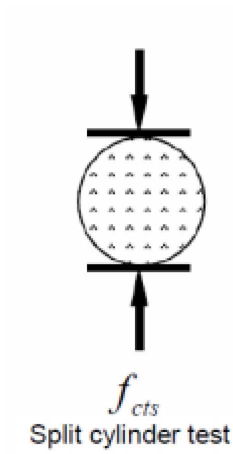

Figure 5.3. Tensile Strength – Splitting Tension [60]

To calculate the approximate tensile strength resulting from the splitting tension test, Equation 5 is used [58].

$$f_t \cong 0.51\lambda\sqrt{f_c'} \tag{5}$$

The third and final method of measuring the tensile strength of concrete is through the modulus of rupture test. Due to the simplicity of the test setup, modulus of rupture test is very common. It can be conducted using three-point bending, as shown in Figure 5.4, as well as four-point bending.

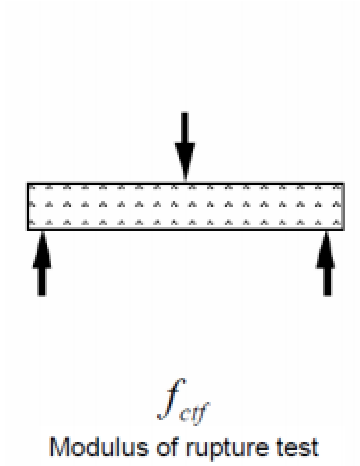

Figure 5.4. Tensile Strength – Modulus of Rupture [60]

The tensile strength during the modulus of rupture testing will yield the highest value when compared to the other two methods and can be calculated using Equation 6.

$$f_t = 0.60\lambda\sqrt{f_c'} \tag{6}$$

For the purpose of the ABAQUS model, the tensile strength of the concrete will be determined using the modulus of rupture equation. Using Equation 6, the tensile strength yields a value of 3.51 MPa. This was deemed an as acceptable value as the general rule of thumb when dealing with reinforced concrete that the tensile strength only yields approximately 5-7% of the compressive strength. It was assumed that the concrete was that of normal density, therefore a value of 1.0 was selected for the density factor, λ.

Plasticity

When defining the plasticity behaviour of concrete, two different behaviours were researched: concrete smeared cracking and concrete damaged plasticity. Concrete smeared cracking is used for monotonic, non-cyclic loading at low pressure. When dealing with this type of plastic behaviour, postfailure tension stiffening properties can be inputted as either a displacement or strain type. Furthermore, the shear retention of the concrete post crack can be defined, allowing for the shear modulus to be reduced once cracking initiates. Although the finite element model is under monotonic loading, concrete smeared cracking is not the ideal plastic behaviour to specify in this scenario. This is due to the fact that the smeared crack concrete model assumes that the act of the concrete cracking is the most important outcome of the plastic behaviour. Also, the cracking behaviour indicates that "cracking [is] the most important aspect of the behaviour, and representation of cracking and postcracking behaviour dominates the modelling" [44].

Concrete damaged plasticity is described as behaviour to model that combines both tensile and compressive properties of the plasticity of concrete. Unlike the smeared cracking model, concrete damaged plasticity is also used when dealing with dynamic loading, although that is not applicable for this project. It takes into account tensile cracking and compressive crushing of concrete when dealing with the material's failure [44]. Therefore, the compressive yield stress as well as the tensile yield stress were the main parameters with this behaviour. The damaged plasticity model for concrete also allows for the compression and tension damage to be specified. For the reasons outlined above, this plastic behaviour model was an ideal choice to use during the construction of the finite element model and its double lap pull out test.

The following list provides a summary of the plasticity parameters of this model.

- Dilation angle, ψ: 36.3
- Eccentricity, ε: 0

- σ_{b0} / σ_{c0}: 1.16
- K_C: 1.0
- Viscosity parameter, μ: 0.08

Due to the limited amount of experimental testing conducted on the concrete test cylinders, the majority of the values noted above were the default input values recommended by Abaqus's User Guide. From literature search, slight adjustments were made to some of the plasticity parameters after several iterations of the model was analyzed.

5.1.2 Steel

As outlined in the Experimental Study portion of this report, the reinforcing used in the concrete prisms was comprised of a single 20M rebar placed in centre of the specimen.

Elasticity & Plasticity

Similar to the concrete material outlined above, the elastic and plastic behaviours of steel were included in order to best represent the material. The elasticity behaviour of steel was modelled as linearly elastic. The Young's modulus of steel was selected at a typical value of 200,000 MPa. Like any other material, this common value was determined through the plastic response of steel during under load, as outlined in Figure 5.5.

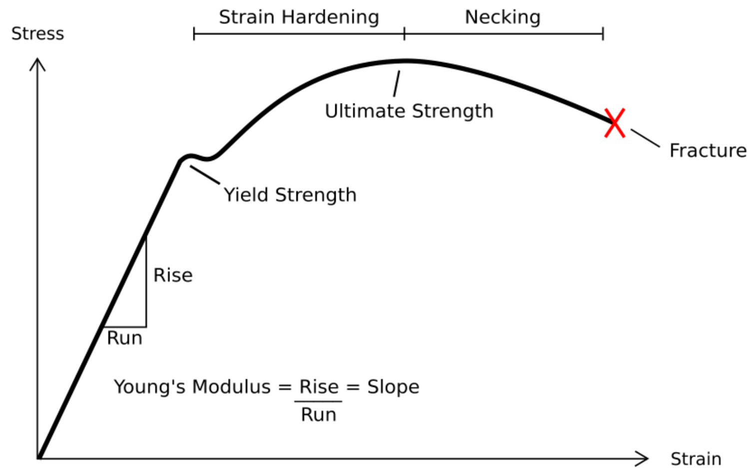

Figure 5.5. Material Response [61]

A Poisson's ratio of 0.3 was used to represent the reinforcing steel. This was chosen as it's a common value used for steel. The plasticity of steel was modelled with a yield stress of 400 MPA and a plastic strain of 0.

5.1.3 CFRP & Epoxy

General

For a number of reasons, the CFRP and epoxy materials were modelled together as one single material, rather than two. The first main reason behind the decision to model the two materials in such a manner comes from the laboratory testing that was previously conducted. In the Experimental Study section, it was explained that the coupon tests were conducted for the CFRP and epoxy materials. As indicated by Atunbi [35], these tensile tests were carried out to measure the properties of the CFRP when paired with the epoxy coating. Therefore, the results obtain from the coupon testing, such as the tensile strength and modulus, are from the coupon of the CFRP sheet saturated with the epoxy. Since the goal of this project is to conduct an accurate replication of the experimental testing, it was decided that taking those properties into account, the test results from the combined CFRP and epoxy, would lead to a better final finite element product. Due to the complexity of the cohesive material and behaviour properties in ABAQUS, additional experimental testing is recommended in order to get best results. This was beyond the scope of this project, as further experimental testing would require additional specimens to be constructed. The second reason of the CFRP and epoxy material combination is due to the complexity of modelling cohesive elements. Modelling an imperfect bond can often result in difficulties in yielding appropriate results. This is mainly attributed to the material properties of cohesive elements as well as proper meshing techniques. The scope of work is focused on completing a successful model replication and looking at the effects of the bond length on the longitudinal strain, ultimate load, and development length. Attempting to properly model the epoxy bond between the CFRP sheet and concrete would be adding a layer of complexity above the goal of this project.

Elasticity & Plasticity

In terms of behaviour, the CFRP sheet and epoxy were modelled to have elasticity and plasticity. For elastic behaviour, a Young's modulus of 37,800 MPa was inputted, which was obtained from the coupon testing. With the relatively recent rise in popularity, a standard Poisson's ratio was not as common as it would be with traditional materials such as concrete and steel. After conducting a literature review of the material, it was found that an acceptable Poisson's ratio for CFRP ranged anywhere from 0.2 to 0.3. Therefore, a value of 0.3 was used. The yield stress of the CFRP and epoxy during its plastic phase was set at 642 MPa, again, from the previous coupon tensile testing.

5.1.4 Summary of Properties

The following table provides an overall summary of the properties inputted into ABAQUS for each material.

Table 5.1. Summary of Model Properties

	Concrete	Steel	CFRP & Epoxy
Type	Isotropic	Isotropic	Isotropic
Young's Modulus (MPa)	25,575	200,000	37,800
Poisson's Ratio	0.2	0.3	0.3
Compressive Yield Stress (MPa)	34.3	400	642
Tensile Yield Stress	3.51	-	-

5.2 Cross-Sectional Dimensions

The dimension of each cross section incorporated into the finite element model can be found in the table below. It should be noted that this was the initial model construction and it was later modelled to incorporate the symmetry of the beam, allowing for a finer mesh. This will be further discussed in Section 5.4.

Table 5.2. Initial Cross-Sectional Dimensions

	No. of Parts	Width	Height	Length
Concrete [1]	2	150 mm	150 mm	500 mm
Steel Rebar [1]	2	300 mm^2 (20M)		500 mm
CFRP & Epoxy [2]	1	100 mm	1 mm	663 mm, 743 mm, 853 mm

Notes:

[1] The length of the concrete and steel rebar correspond to only one specimen, not the entire length of the test setup

[2] The three different lengths corresponding to the CFRP and epoxy is due to the varying bond lengths (160 mm, 240 mm, 350 mm). This incorporates the 500 mm from the first concrete prism, the 3 mm gap between the two prisms, and the bond length.

The entire length of the test setup, as described in the Experimental Study section, would be a total of 1003 mm. This includes the two 500 mm long concrete beams, with a 3 mm gap separating the specimens. The length of the CFRP sheet and application of the epoxy vary due to their respective bond lengths. Again, this was constructed in a fashion to ensure the experimental test setup was simulated as accurately as possible.

A visual representation of the constructed ABAQUS model can be seen in Figure 5.6.

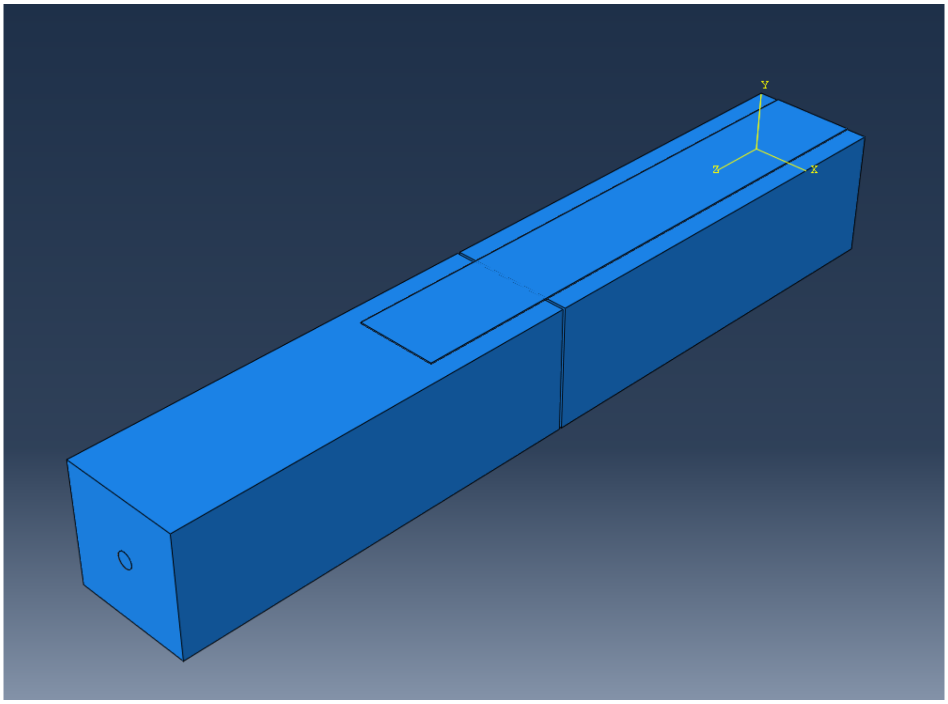

Figure 5.6. Constructed ABAQUS Model

5.3 Elements

5.3.1 General

The construction of an ABAQUS model requires the creation of parts. These parts, which essentially make up the entirety of the model, are assigned to be specific element types, which is dependent on what is being modelled. Below are the five main aspects of elements that affect the outcome of the model.

- Family;
- Degrees of freedom;
- Number of nodes;
- Formulation; and,
- Integration.

Family

When using ABAQUS, each individual part that is modelled is assigned to an element family, which is commonly known as an element type. Given the complexity of the program, ABAQUS has several different element types that can be used during an analysis, each of which is relevant and assigned to the specific part you are modelling. Dependent on what the context of the model is, a single element type of element can be used for the entire model, or several. The more common element types, for example, can be viewed in Figure 5.7 [44].

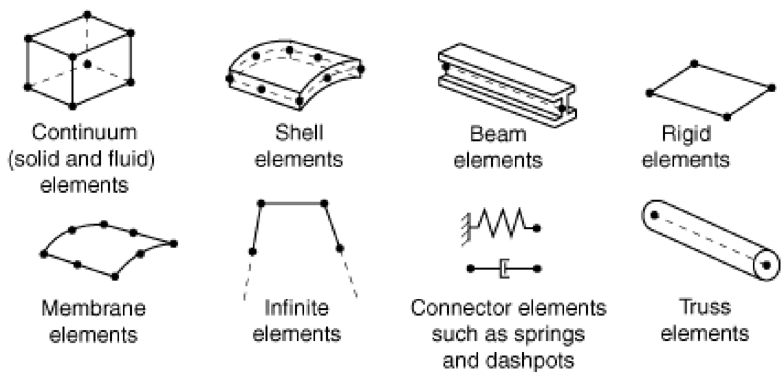

Figure 5.7. Common Element Types [44]

Degrees of Freedom

Within each element family, the degrees of freedom are set and cannot be modified. Therefore, the degrees of freedom may be the translation, rotation, or temperature at each individual node, depending on the which element family was selected.

Nodes

When selecting the specifics of each element, the number of nodes desired can lead to further refinement of the model. Essentially, the number of nodes can alter the model's output, as the interpolation technique is directly related, subsequently affecting the results. Modelled parts with nodes existing only at each corner, such as a square with four nodes, will use linear interpolation with respect to each node. This is called a linear element. When a part is modelled with a node in each corner as well as midspan nodes, such as a square with eight nodes, quadratic interpolation will be used. This is called a quadratic element. Depending on the desired level of accuracy, the number of nodes and their respective interpolation methods can be changed. Although quadratic elements are deemed to be more accurate, this is not always ideal, as an increased number of nodes has a positive correlation with the model's run time. Therefore, attempting to analyze large models consisting of many nodes with quadratic interpolation can result in difficult and lengthy processing times.

Figure 5.8 shows an example outlining the differences between a linear and quadratic element.

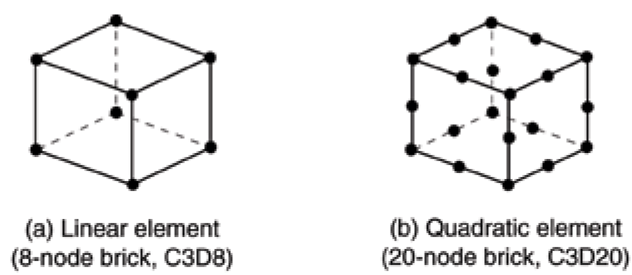

Figure 5.8. Linear & Quadratic Elements [44]

Formulation & Integration

The formulation of an element, as defined in [44], is the procedure used in defining the behaviour of said element. Based on the element type selected within ABAQUS, several different formulations are possible. The User Manual states that ABAQUS uses lumped mass formulation for what is considered a low-order element, which leads to allowing the second mass moment of inertia to deviate from its theoretical values. Similar to the formulation of an element, the integration can be modified to full or reduced integration elements, depending on the element selected.

5.3.2 Modelled Elements

Solid Elements

The solid element in ABAQUS is considered the standard element and is often paired with homogeneous material to conduct both linear and non-linear analysis. Furthermore, the solid element can experience large deformation during the analysis but may lead to not as accurate results if distortion of the element is implemented. The solid element includes both linear and quadratic interpolation options as well as full and reduced integration.

The main issues that can potentially arise when analyzing a model with solid elements are known as hourglassing and shear and volumetric locking. Hourglassing most often occurs when a first-order, or linear, reduced integration method is used. Described by the Abaqus Analysis User’s Guide [44], the problem will arise due to an element having just a single integration point, which can distort the model in such a manner that the strains at the integration points are determined as zero at the integration points. This, unfortunately, “leads to uncontrolled distortion of the mesh” [44]. There are, however, a number of way to mitigate hourglasssing issues. By selecting the second-order, or quadratic, reduced integration method, the model will have very little difficulties in producing acceptable results. Therefore, it is recommended to use second-order reduced integration as the geometric order when possible.

Shear and volumetric locking can occur to elements subjected to full integration. Shear locking occurs when the element's resulting displacement is extremely underestimated indicating that it is too stiff [62]. Therefore, this phenomenon occurs with elements subjected to bending. Volumetric locking occurs when the resulting behaviour of a material is incompressible. This can also occur in thinly constructed shell elements.

Similar to the hourglassing issue, the effects of shear and volumetric locking can oftentimes be mitigated through the element's specified integration method. This locking behaviour, however, can be prevented by using first-order elements with selective reduced integration. This is the opposite when compared to the hourglassing prevention, as it requires second-order elements. Therefore, there is often a certain level of adjustment when dealing with solid elements in determining their order level as well as their integration method.

Both the concrete and the steel reinforcing rebar were modelled as a three-dimensional (3D) deformable solid elements. This includes an 8-node linear brick, reduced integration with hourglass control geometry (C3D8R).

Shell Elements

The shell element is considered a structural element and is used to model parts in which the measured thickness is extremely small when compared to the other dimensions. Much like a solid element, shell elements have both linear and quadratic interpolation method. The majority of shell elements, however, use a reduced integration in order to provide more accurate results and a reduced analysis time. They are also susceptible to hourglassing, which needs to be monitored when using first-order elements.

The CFRP and epoxy combination were modelled as a shell element. This includes a 4-node doubly curved thin shell, reduced integration with hourglass control geometry (S4R).

Cohesive Elements

Cohesive elements are used to model a bond between two interfaces. The cohesive can be modelled as an element susceptible to deformation or completely rigid and is often modelled to have both of its surfaces tied to another part or component. Cohesive elements are often tied to other elements through tie constraints and can produce varying responses, depending on the desired outcome of the cohesive effects. If the epoxy layer bonding the CFRP sheet to the reinforced concrete prism as a separate component, a cohesive element would be utilized. Due to a variety of factors, as discussed in Section 5.1, the epoxy was modelled with the CFRP as one single part, thus alleviating the need to model a cohesive element.

Summary

The table below provides a summary of the elements incorporated into the model, including the type, node shape and number, and integration method used.

Table 5.3. Summary of Elements

	Concrete	Steel Rebar	CFRP & Epoxy
Family/Type	3D Stress	3D Stress	Shell
Element Shape	Hex	Hex	Quad
Technique	Sweep	Sweep	Structured
Integration	Reduced	Reduced	Reduced
Element	C3D8R	C3D8R	S4R

5.4 Boundary Conditions

Boundary conditions have a crucial role not only in finite element analysis, but in the entirety of mathematics. They are necessary in specifying to desired solutions, as they provide a method of constraints to the problem. In finite element modelling, boundary conditions have a variety of abilities, but are typically used in constraining displacements and rotations of the model. On a more detailed level, boundary conditions can be used in fluid, pore, and acoustic pressures, as well as temperatures to name a few. Therefore, defining the appropriate boundary conditions in ABAQUS is critical, as they have a significant impact on the model's analysis.

For the purpose of this model, two different types of boundary conditions were used: displacement/rotation and symmetry. A displacement/rotation boundary condition of U3 = 1 was used for displacement load applied to the rebar. This was used in conjunction with the specified amplitude to simulate the 0.5 mm/min loading. In order to ensure displacement did not occur at the opposite end of the loading, a second displacement/rotation boundary condition of U1 = U2 = U3 = 0 was used. The symmetry boundary condition was used along the model's axis of symmetry. This is further discussed in Section 5.4.1.

5.4.1 Symmetry

Due to the complexity in simulating a double lap shear pull out test in a finite element software, the model requires a high level of computing power and time. Aside from the meshing, increment size, and output requests, the model can be analyzed more efficiently by introducing symmetrical boundary conditions. When applicable, the symmetry boundary conditions allow users to make use of the plane of symmetry.

Abaqus allows users to choose between symmetry, antisymmetry, and encastre boundary conditions. When selecting the symmetry condition, the following options are presented [44]:

- **XSYMM**: Symmetry about the x-axis (U1 = UR2 = UR3 = 0);
- **YSYMM**: Symmetry about the y-axis (U2 = UR1 = UR3 = 0); and,
- **ZSYMM**: Symmetry about the z-axis (U3 = UR1 = UR2 = 0).

Due to the orientation of the model, the XSYMM boundary condition was used. The line of symmetry of the constructed model is shown in Figure 5.9.

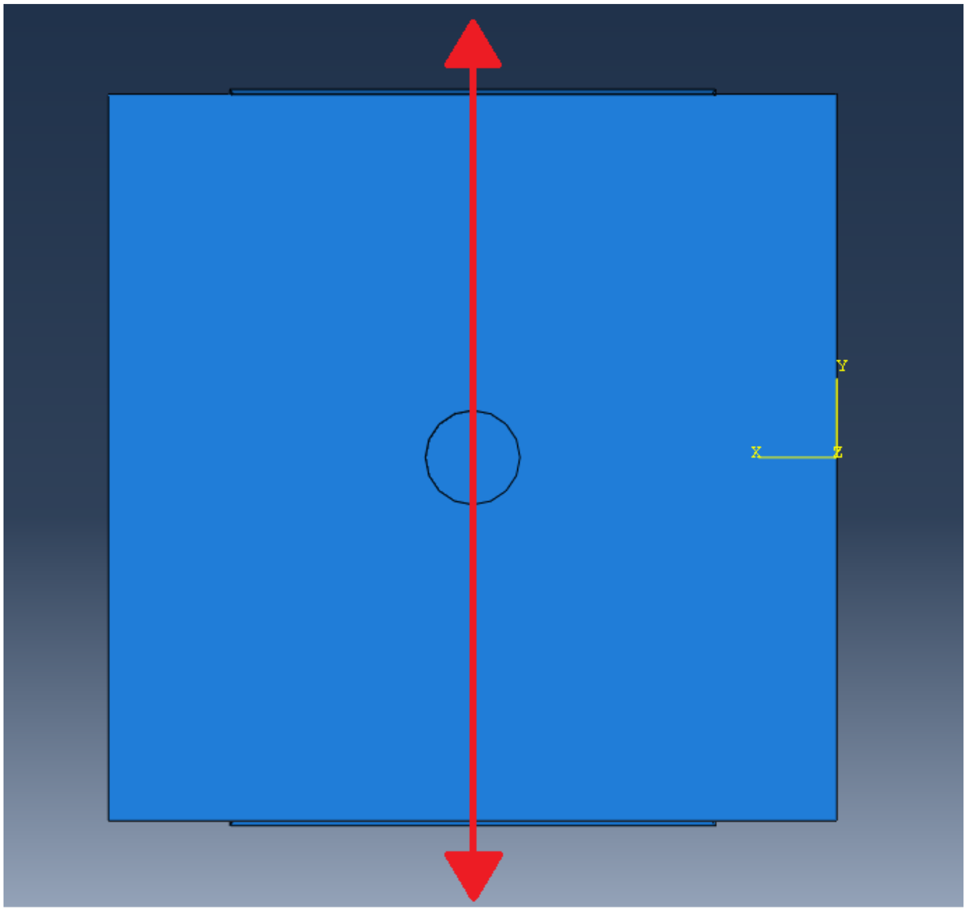

Figure 5.9. Line of Symmetry (XSYMM)

In order to apply the symmetry boundary conditions, half of the model was reconstructed about the x-axis. The updated model dimensions can be found in the following table.

Table 5.4. Cross-Sectional Dimensions with Symmetrical BCs

	No. of Parts	Width	Height	Length
Concrete [1]	2	75 mm	75 mm	500 mm
Steel Rebar [1]	2	150 mm^2 (½ 20M)		500 mm
CFRP & Epoxy	1	50 mm	1 mm	160 mm, 240 mm, 350 mm

Notes:

[1] The length of the concrete and steel rebar correspond to only one specimen, not the entire length of the test setup

Using the new cross-sectional dimensions, Figure 5.10 shows the newly constructed model. Note that the symmetry boundary conditions (XSYMM) are also visible in the figure.

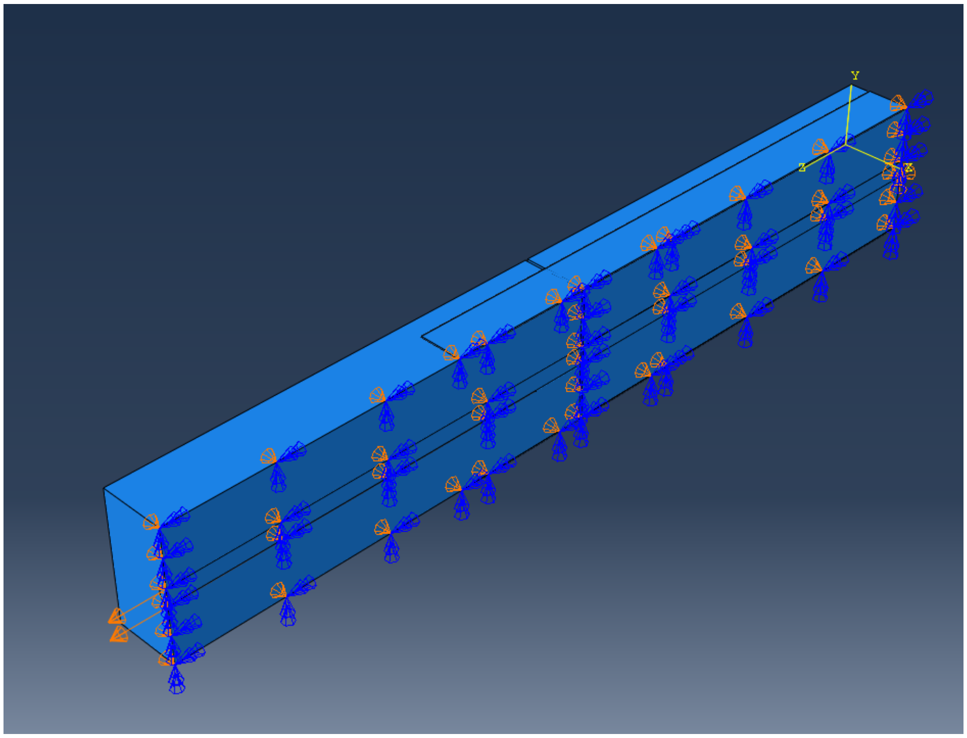

Figure 5.10. Symmetry Boundary Conditions

5.4.2 Constraints

ABAQUS allows the user to specify a number of different constraints to an instance, which include:

- Multi-point constraints
    - Linear equation
    - Multi-point
    - Kinematic coupling
- Surface-based constraints

- Mesh tie
- Coupling
- Shell-to-solid coupling
- Fasteners

- Embedded elements

To ensure a realistic interaction between two parts or instances occur, proper constraints must be implemented. The two parts with constraints incorporated are the steel rebar and CFRP sheet, which both utilized a surface-based tie constraint. A basic visual explanation of a tie constraint can be seen in Figure 5.11.

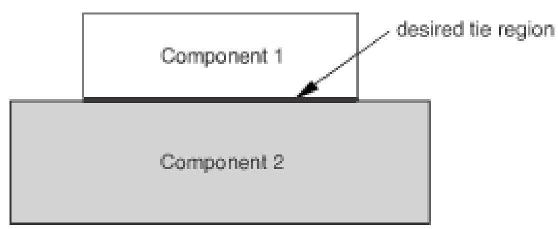

Figure 5.11. Surface-based Tie Constraint [44]

For the steel rebar, using a tie constraint is not typical as reinforcement is most commonly constrained as an embedded element. The decision to model it as a tie constraint was due to the parameters involving the rebar. Since it was modelled as a protruding element, applying an embedded constraint to the rebar was not possible and will result in a constraint error. Due to the ABAQUS and its solving algorithms, a part cannot be constrained as embedded in another if a portion of said part lies outside of its host, such as the protruding rebar. Although modelling the rebar fully inside the concrete prism and not protruding at all was investigated, it was determined that using a tie constraint and allowing the rebar to extend past the concrete prims was the better decision. The main reason is due to the experimental test setup, as illustrated in Section 3.2, which reflects the rebar protruding from each end of the concrete prism. Although this was done only to provide a method in which the testing apparatus can attach to the specimen, it was nonetheless included in the model construction. With the displacement load's point of contact being the rebar, it was important to follow suite with the model, rather than applying the displacement load over the entire end area of the concrete prism, which would have been required with an embedded rebar.

Much like the reinforcing steel, the surfaced-based meshing tie constraint was implemented for the CFRP and epoxy element to the concrete. Although other constraints were investigated, the tie constraint was the more appropriate option.

Table 5.5. Constraints

Location	Type	Master Surface	Slave Surface
Steel Rebar	Surfaced-based: Mesh Tie	Steel Rebar	Concrete
CFRP Sheet	Surfaced-based: Mesh Tie	Concrete	CFRP Sheet

5.5 Loading

The experimental testing was performed using the double lap pull-out test, which was the testing method recommended in CSA S806-12 to use when investigating the bond behaviour FRP-concrete interface. The goal of this project is to simulate the test setup; therefore, the double lap pull-out test was simulated in ABAQUS. Due to the nature of the software, this was performed by setting a displacement boundary condition on each end of the concrete specimens. A displacement rate of 0.5 millimeters per minute on one end was applied to the model along the z-axis, displacing the concrete prims until failure of the bond was achieved. The other concrete prism was pinned against movement in the z-axis, allowing no displacement. In order to effectively achieve failure of the model, sufficient displacement had to be ensured. The following table is an example amplitude assigned to the model to simulate a 0.5 mm/min displacement.

Table 5.6: Displacement Load Amplitude

Time/Frequency (seconds)	Amplitude (mm)
0	0
60	0.5
120	1
180	1.5
240	2
300	2.5
360	3
420	3.5
480	4.0
540	4.5
600	5.0

5.6 Mesh Sensitivity Analysis

In order to perform the analysis, the model must be meshed. While meshing can appear to be a very simplistic task, it can be highly sensitive in developing proper meshing technique to acquire accurate results. Some of the meshing factors that affect the outcome of a model include the element's shape as well as the specific meshing technique chosen. Depending on the instance or part that is being meshed, the complexity of the meshing increases as the intricacy of the part's geometry increases. The general meshing procedure, however, is relatively straight forward for each scenario. The standard approach is to commence with assigning seeds to each part, which ultimately determine the size of the mesh. To assign seeds to a part, a global size number must be inputted, which represents the number of mesh elements per millimetre. Therefore, a small number specified for the global size will create a high number of seeds for the part, resulting in a finer level of mesh. Once the proper amount of seeds is designated, the mesh will be assigned to all parts of the model. This can be conducted by part or instance, dependent on whether or not the assembled instances are declared independent or dependent.

In order to determine an appropriate mesh size, a basic mesh sensitivity analysis was performed. Since several iterations of the model with varying mesh sizes needed to be analyzed, a scaled down model was constructed. Symmetry boundary conditions were also applied to further reduce the model size, resulting in a shorter run time.

For the mesh sensitivity analysis, four different mesh sizes were analyzed, including: 12 per mm, 11 per mm, 10 per mm, and 9 per mm. Note that the mesh size denotes number of elements per millimetre. Figure 5.12 represents the mesh sensitivity analysis performed, which provides a visual indication of when convergence occurred. This was done for a scaled down version of the CFRP sheet with a bond length of 160 mm.

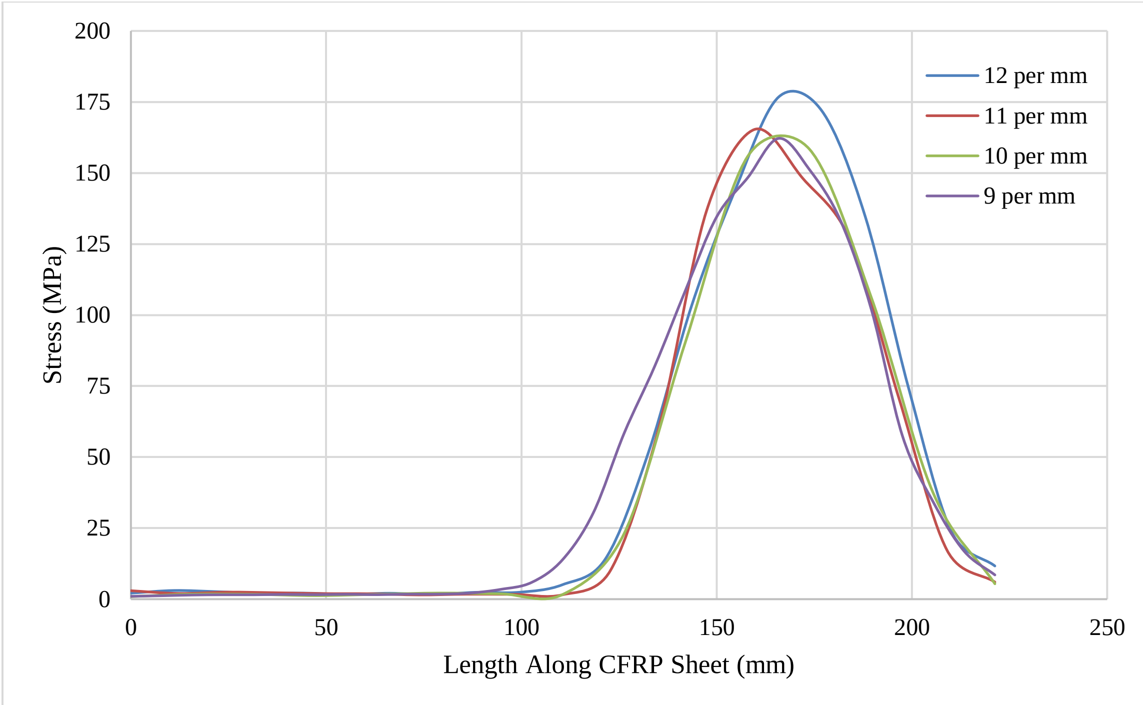

Figure 5.12. Mesh Sensitivity Analysis

From Figure 5.12, it is evident that as the mesh size reduces, the stress along the length of the CFRP sheet begins to converge. The 12 per mm mesh size yields a slightly higher maximum stress value while the other three mesh sizes do not vary significantly in comparison to one another. Therefore, a mesh size of 10 per mm was deemed appropriate and chosen for the full finite element model.

6.0 NUMERICAL MODEL RESULTS AND DISCUSSION

6.1 General

The results of the finite element model analysis of the specimen is presented in this chapter. For this project, the specimens with the three varying bond lengths from the experimental study was simulated in ABAQUS. This includes a bond length of 160 mm, 240 mm, and 350 mm. Included in the results are the maximum loads experienced by the whole model during the analysis as well as the maximum strain experienced by the CFRP sheets. With the strain results of the CFRP sheet, the development length is determined and discussed in comparison with theoretical values. Finally, the results obtained from the finite element model will be compared to the results of the previously conducted experimental study.

6.2 Development Length & Maximum Tensile Strain

To compare the numerical model results, the appropriate theoretical values for development length and maximum tensile strain were determined using CSA S806-12, Design and construction of building structures with fibre-reinforced polymers. As per Clause N.3.2.7 (Annex N) of CSA S806-12, the effective length, or development length, can be determined using the following equation:

$$L_e = \frac{25\,350}{\left(t_f E_f\right)^{0.58}} \tag{7}$$

Where t_f and E_f represent the thickness and modulus of elasticity of the FRP sheet, respectively [30]. Using the Equation 7, a theoretical development length of 56.4 mm is calculated, which incorporates a FRP sheet thickness of 0.165 mm with a modulus of elasticity of 227 GPa [47].

To determine a theoretical maximum tensile strain value, Equation 8 was used, as per Clause 11.3.1.3 of CSA S806-12.

$$\varepsilon_{fmax} = 0.41\sqrt{\frac{f_c{}'}{n_f E_f t_f}} \leq 0.007 \tag{8}$$

Where t_f and E_f represent the thickness and modulus of elasticity of the FRP sheet, respectively, f_c' is the compressive strength of the concrete, and n_f is the number of FRP plies (layers). By using Equation 8, ε_{fmax} exceeds the limit of 0.007. Therefore, for this project, the theoretical maximum tensile strain will be taken as 0.007.

6.3 Model Results

The following results are based on the finite element models constructed in ABAQUS. As previously mentioned, a perfect bond was assumed at the CFRP-concrete interface.

6.3.1 Bond Length of 160 mm

The total length of the CFRP sheet in the first model analysis is 663 mm. This consists of the sheet bonded along the first concrete specimen of 500 mm, the 3 mm gap between the two concrete specimens, and 160 mm onto the second concrete prism. The total time to analyze the model was 10.17 hrs.

Upon completing the analysis, the total force exerted on the model was investigated. As per the experimental testing, the load was applied as a displacement load on the rebar. Therefore, the total force experienced by using the following relationship:

$$F = \sigma * A \tag{9}$$

Where σ and A represent the stress and the cross-sectional area of the rebar, respectively. Figure 6.1 shows the model's load versus time curve.

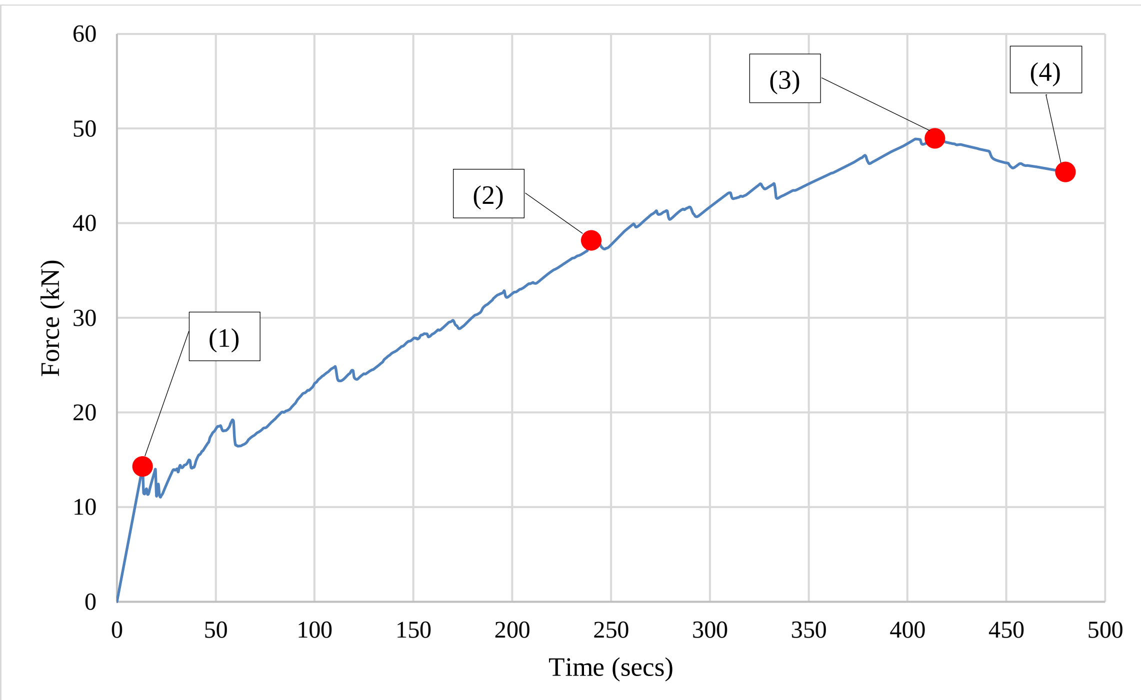

Figure 6.1. Load vs. Time – 160 mm Bond Length

From Figure 6.1, the initial loading of the model creates a linear force slope for the first 15 seconds of the analysis, as indicated by point (1). Upon reaching this peak, there is a small decrease in force but continues to slope continues to follow a positive linear path. Point (2) occurs at the 240 second mark of the analysis, representing the halfway point of the model's total run time. The force at point (2) is 38.2 kN, which is approximately 78% of the maximum force. Point (3) represents the maximum force obtained from the 160 mm bond length is 49.0 kN. This occurs at the 414 second mark of the analysis. After reaching point (3), the slope of the force diagram begins to decrease until reaching the end of the analysis at point (4). The reduction in the force indicates that failure has occurred in the model. The total time period of the analysis was 480 seconds.

Figure 6.2 shows the plot of the longitudinal strain along the bond length of the CFRP sheet. The strain values were derived from a path line positioned in the middle of the CFRP sheet within ABAQUS. At the start of the bonded length, the strain of the CFRP sheet is at its maximum of 0.0058, where it decreases linearly for 30 mm along its length until reaching a strain of 0.0045. For the next 90 mm along the bonded length, the strain values continue on a very slight decline, which indicates debonding occurring at the CFRP-concrete interface. As the strain continues along the bonded length past this point, a sharp decline occurs before reaching zero.

The strain values along the 160 mm bond length were taken from the model prior to the sheet fully debonding from the concrete. This plot was also used in determining the development length, or effective length, of the CFRP sheet. From Figure 6.2, the approximate development length of 37.4 mm was obtained by measuring the elastic region of the curve, which is the portion consisting of the linear decreasing slope. In Section 6.2, a theoretical development length of 56.4 mm was calculated based on similar FRP sheet properties. Therefore, a 40.5% difference between the theoretical and numerical model length was determined.

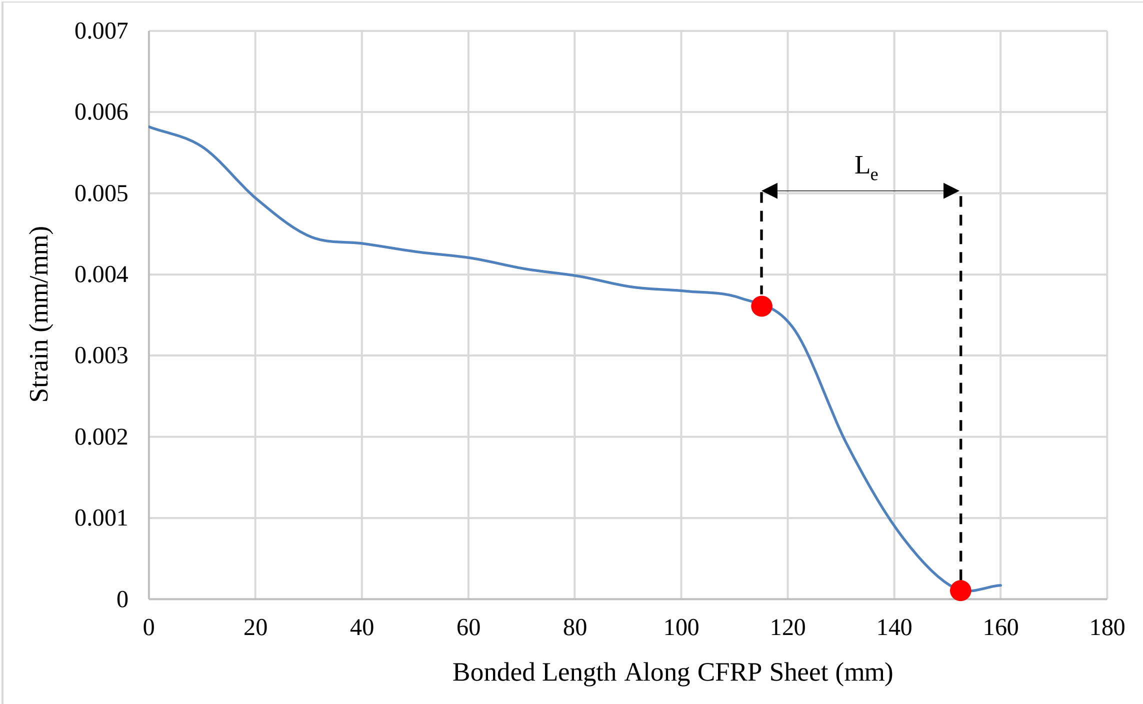

Figure 6.2. Strain vs. Bond Length Along CFRP Sheet – 160 mm Bond Length

6.3.2 Bond Length of 240 mm

The total length of the CFRP sheet in the second model analysis is 743 mm. This consists of the sheet bonded along the first concrete specimen of 500 mm, the 3 mm gap between the two concrete specimens, and 240 mm onto the second concrete prism. The total time to analyze the model was 14.91 hrs.

Figure 6.3 displays the force in the system due to the 0.5 mm/min loading. Similar to the 160 mm bond length model, the initial force creates a steep slope for the first 15 seconds of the analysis until reaching point (1). The force continues to increase with a more gradual slope leading to a plateau until reaching point (2) at 41.3 kN, which represents the halfway point of the analysis. There is a slight increase in the slope for the following 106 seconds until reaching the maximum at point (3). The maximum force obtained from the 240 mm bond length is 49.2 kN, occurring at 435.5 seconds. Following point (3), the force begins to reduce for the remainder of the analysis. Point (4) represents the end of the 240 mm bond length analysis, which is at a time period of 660 seconds.

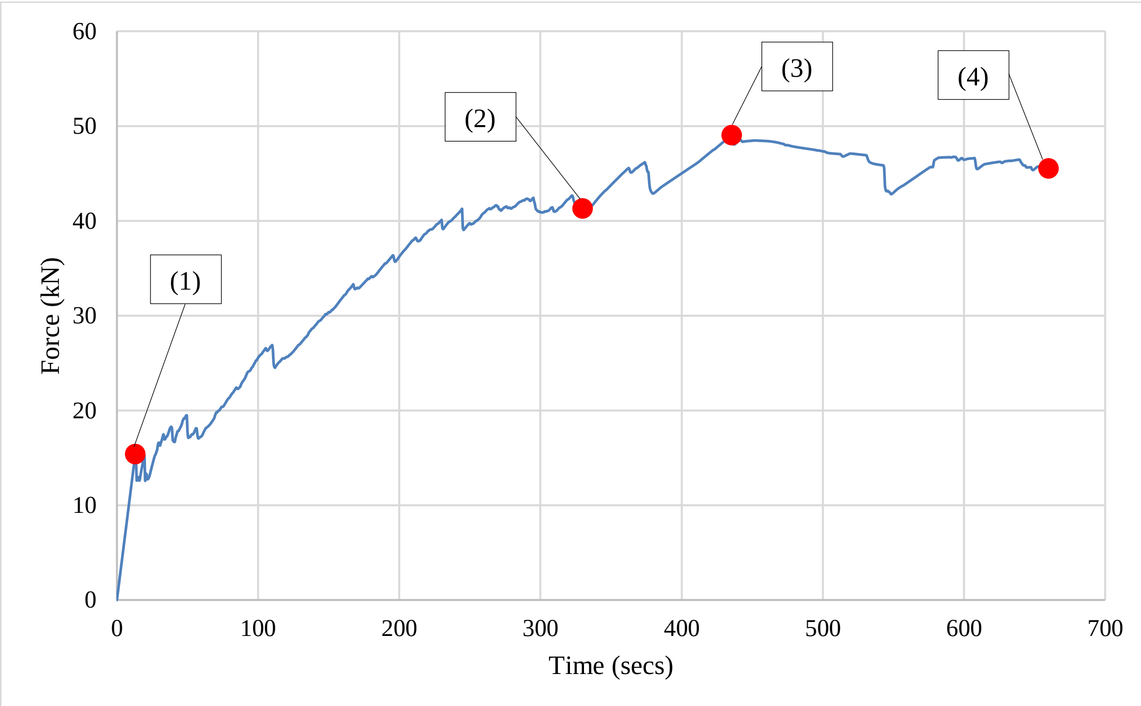

Figure 6.3. Load vs. Time – 240 mm Bond Length

Figure 6.4 shows the plot of the longitudinal strain along the bond length of the CFRP sheet from a path line positioned in the middle of the sheet. The strain at the start bonded length is at its maximum of 0.0075. This exceeds the theoretical maximum tensile strain value of 0.007 as defined by Clause 11.3.1.3 of CSA S806-12. Similar to the 160 mm bond length, the strain values decrease linearly along the bonded length until reaching a small plateau at approximately 190 mm along the CFRP sheet. Next, the strain values decrease significantly over the development length portion of the graph before reaching zero.

The strain values along the 240 mm bond length were taken prior to full debonding of the CFRP-concrete interface. As noted above, the development length of the sheet is shown in Figure 6.4, which was approximated at 31.3 mm. Again, this was determined by measuring the elastic region of the curve prior to debonding of the interface. The 240 mm bond length model yielded a 57.8% difference in length when compared to the theoretical development length.

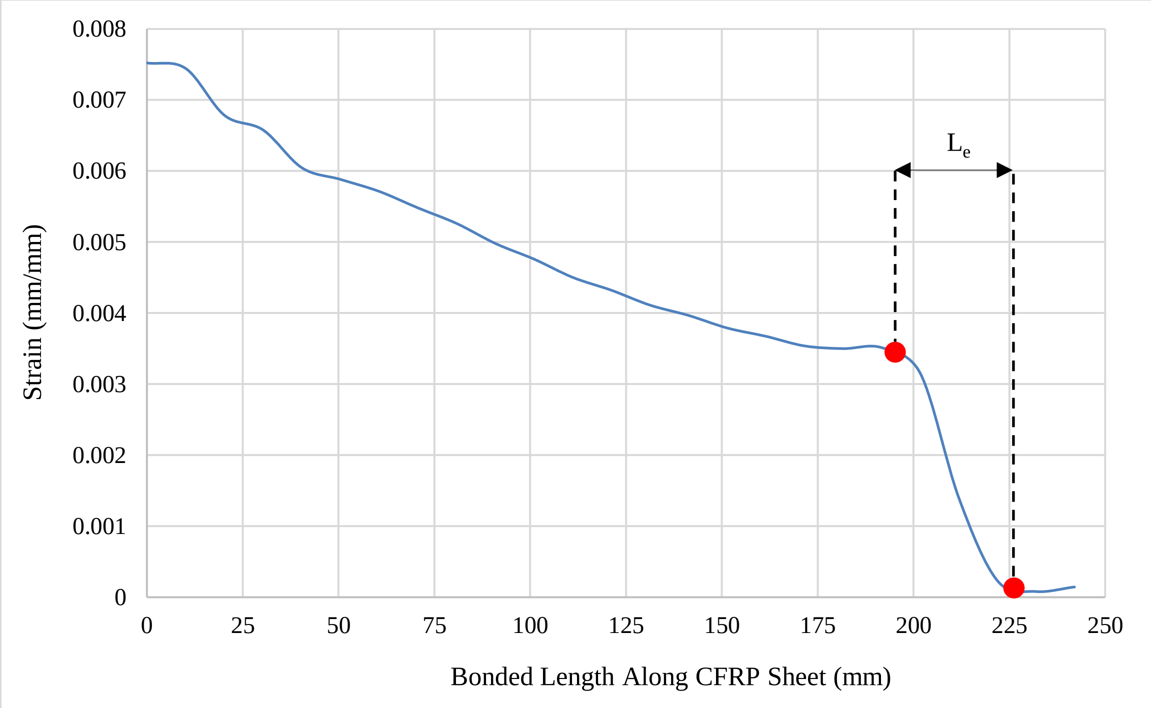

Figure 6.4. Strain vs. Bond Length Along CFRP Sheet - 240 mm Bond Length

6.3.3 Bond Length of 350 mm

The third and final model consists of an 853 mm long CFRP sheet. This includes the sheet bonded to the first concrete specimen of 500 mm, the 3 mm gap between the two concrete blocks, and the 350 mm bonded length onto the second concrete block. The total time to analyze the model was 21.10 hrs.

The force due to the 0.5 mm/min displacement loading of the 350 mm bond length model can be seen in Figure 6.5. As with the other two models, the force curve from the model follows a similar trend. For the initial 15 seconds, the applied load created a linear slope in the force curve, until reaching point (1) at 16 kN. Upon reaching this mark, the load continues to increase, resulting in a linear increase in force. The maximum force, point (3) occurred just after reaching the halfway point in the analysis, point (2). The ultimate load of the model is 51.9 kN, which occurs at 396.5 seconds. Following this peak, the force curve begins to decrease before reaching a plateau for the remainder of the analysis. Point (4) represents the termination of the 350 mm bond length analysis, which is at a time period of 780 seconds.

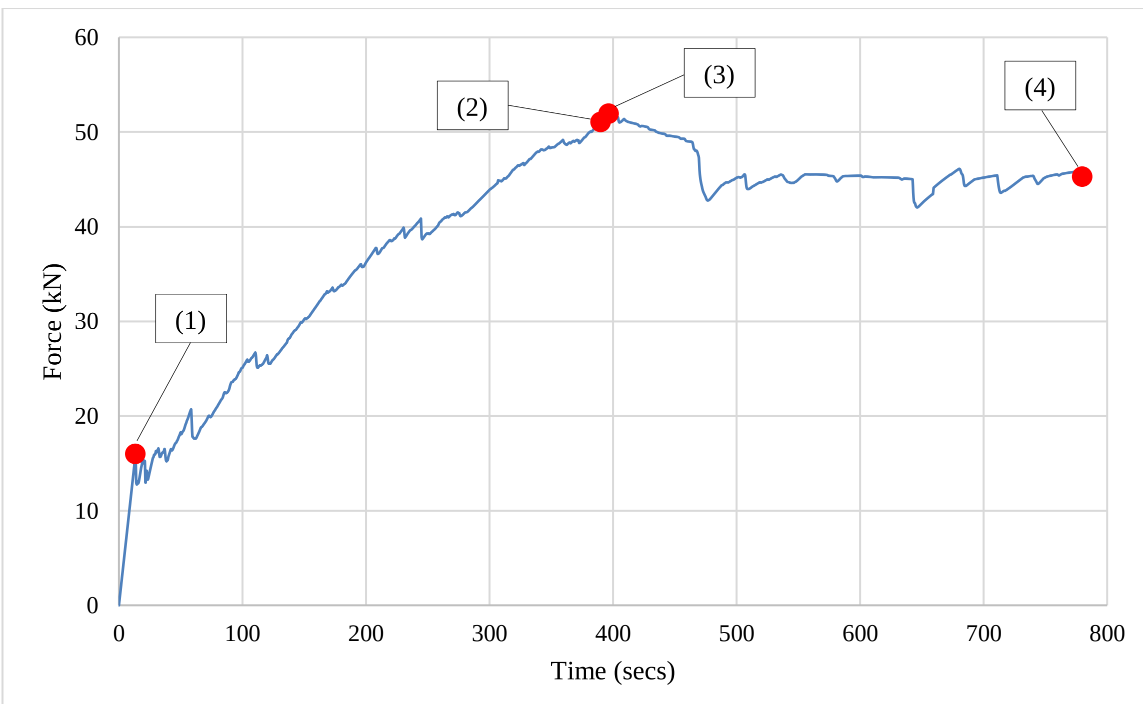

Figure 6.5. Load vs. Time – 350 mm Bond Length

From Figure 6.6, the maximum longitudinal strain of 0.0090 was measured at the start of the bond length. Similar to the 240 mm bond length model, this exceeds the theoretical maximum strain value of 0.007. The strain in the CFRP sheet decreases along the bonded length for the first 40 mm, before reaching an increase followed by a sharp decrease. Next, the longitudinal strain continues to decrease, matching the slope of the first section. This continues until reaching the elastic region of the graph, which eventually reaches zero strain at the end of the bond length at 350 mm.

The longitudinal strain values along the 350 mm bond length were taken prior to full debonding of the CFRP-concrete interface. The development length of the CFRP sheet, determined from the elastic region of the curve in Figure 6.6, was measured to be approximately 39.1 mm. This was lower than the theoretical development length of 56.4 mm, resulting in a 36.2% difference.

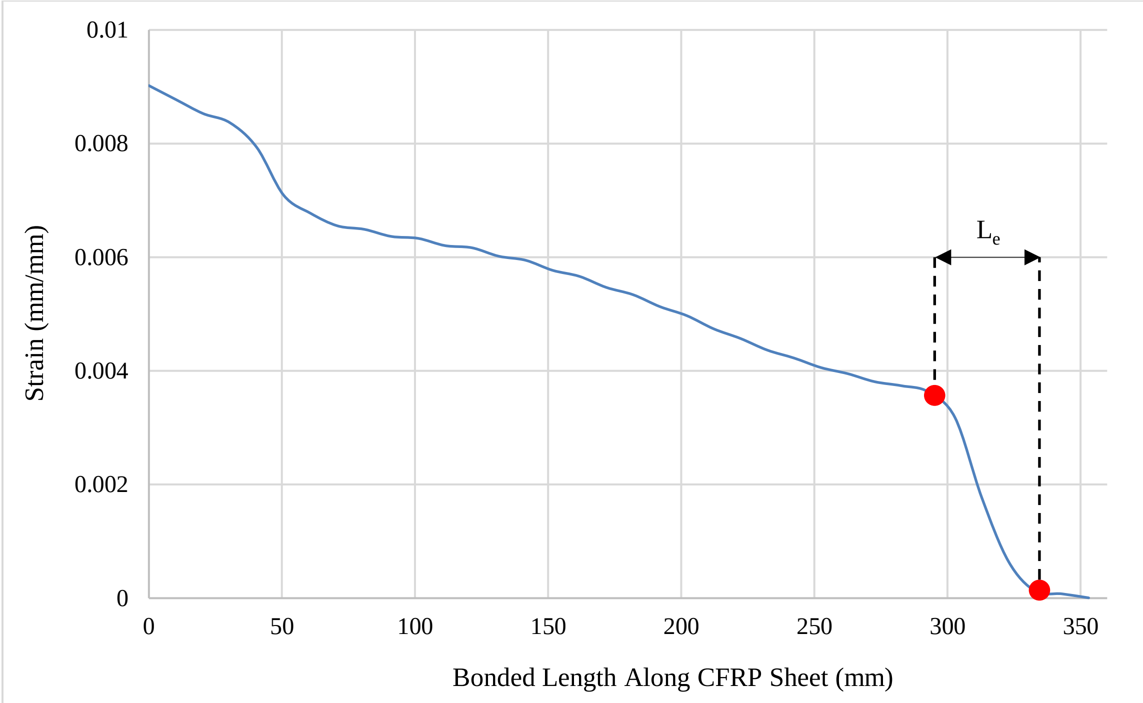

Figure 6.6. Strain vs. Bond Length Along CFRP Sheet - 350 mm Bond Length

6.3.4 Summary of Results

The following table provides a summary of the results obtained from the 160 mm, 240 mm, and 350 mm bond length model analyses. This includes the total run time of the models, the maximum loads, longitudinal strains, and development lengths.

Table 6.1. Summary of Model Results

Result	Total Run Time	Maximum Force	Maximum Strain (mm/mm)	Development Length
160 mm	10.17 hrs	49.0 kN	0.0058	37.4 mm
240 mm	14.91 hrs	49.2 kN	0.0075	31.3 mm
350 mm	21.10 hrs	51.9 kN	0.0090	39.1 mm

The results obtained from each of the bond length models show that an increase in bond length does not result in a significant increase to the maximum force. In comparing the 160 mm bond length to the 240 mm bond length, the ultimate load saw a minimal increase of 0.4 %. The maximum force of the 350 mm bond length was slightly higher, yielded an increase of 5.9 % and 5.5 % when compared to the 160 mm and 240 mm bond length, respectively. As noted previously, the displacement load applied to the models was at the same loading rate of 0.5 mm/min. Due to the nature of the finite element software, a time period large enough to ensure failure occurred had to be specified. Therefore, a total time period for each bond length was chosen based on the experimental study. This was not necessary as failure occurred for each model prior to reaching the 500 second mark.

The maximum strains of the 240 mm and 350 mm bond length models were 0.0075 and 0.0090, respectively. These values are higher than the theoretical maximum tensile strain of 0.007, calculated from Equation 8. Higher strain values were expected in the models when compared to the experimental and theoretical values due to the finite modelling parameters. The experimental study previously completed as well as literature review notes that the main limiting factor in CFRP sheets externally bonded to reinforced concrete is the CFRP-concrete interface. Since a perfect bond at the CFRP-concrete interface was used, the epoxy was not modelled as a separate cohesive material. Therefore, the capacity of the system changes from the epoxy to the CFRP sheet itself, which would undoubtedly yield a higher strain value.

Based on the longitudinal strain diagrams, it can be concluded that the three bond length models failed due to debonding of the CFRP sheet from the concrete prism. The development length of each model was measured from the elastic region of the longitudinal strain curve. The theoretical development length value, determined from Equation 7, was calculated to be 56.4 mm. Results obtained from the models were slightly lower than this value, with all three development lengths in the 30 mm range.

6.4 Comparison to Experimental Results – 160 mm Bond Length

The finite element model was modelled to simulate the experimental study previously done by Atunbi [35]. As such, the results obtained from the model will be compared to the results o the experimental study. For this project, the results from 160 mm bond length specimen will be used in the comparison.

From Figure 6.7, the loading of the CFRP sheet externally bonded to reinforced concrete yield different paths between the two results. The results from the model has a significant initial loading force before continuing on a gradual slope in comparison to the experimental results, which yields a much more constant and gradual slope from the initial start up until reaching its maximum loading force. As noted in Section 6.3.1, the ABAQUS model reached a maximum force of 49.0 kN at 414 seconds. The maximum force of the experimental specimen was slightly lower at 41.5 kN, which occurred at the 388.4 second mark during the testing. Upon reaching its maximum forces, the experimental test has a significant decrease in force, followed by a slight increase before reaching a sudden failure. For the model, however, the force begins decreasing linearly before reaching the end of the specified analysis time.

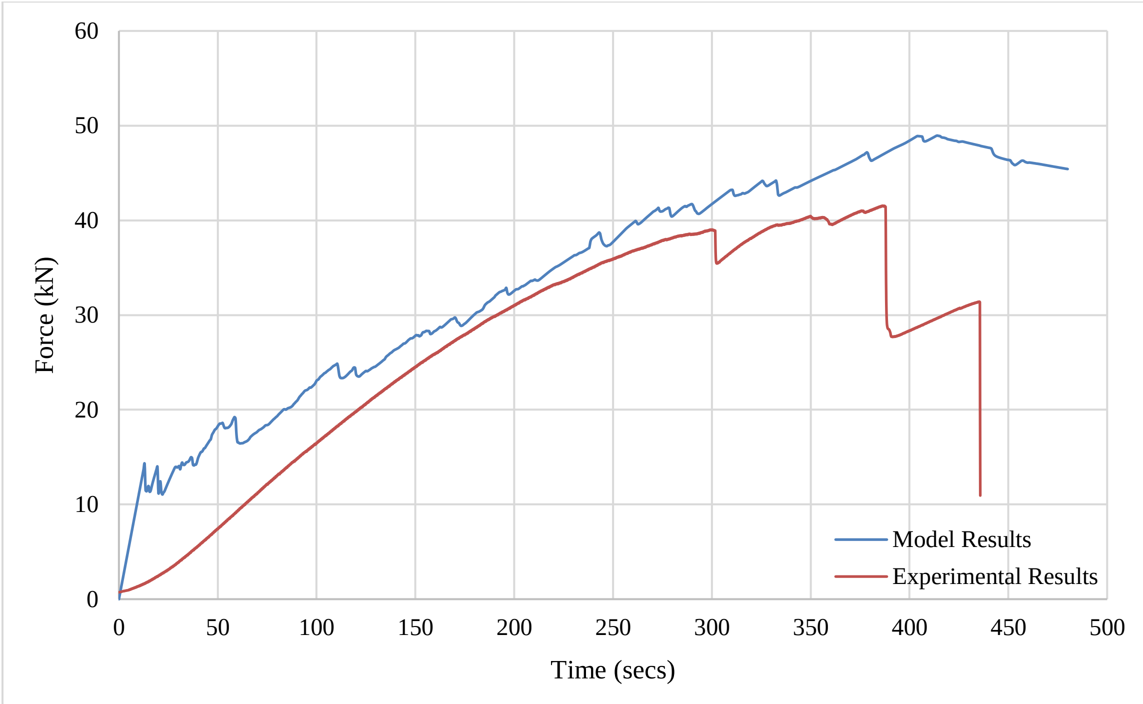

Figure 6.7. Load vs. Time Result Comparison

Figure 6.8 outlines the comparison in longitudinal strain along the 160 mm bonded length of the CFRP sheet. The experimental results show an initial maximum strain value of 0.0054, which continues on a relatively flat slope before reaching the elastic region of the curve. From the ABAQUS model results, the initial strain is slightly higher with a value of 0.0058. For the model results, however, the portion of the curve prior to the elastic region is not entirely linear, as it decreases over the first 25 mm before reducing to a less significant slope. Both curves experience an elastic region, indicating that the CFRP sheet remains bonded to the concrete and allows for the development length to be determined. The longitudinal strain of the ABAQUS model has an approximate development length 37.4 mm while the experimental testing has a slightly larger length at 40 mm. Both of these values are lower than the theoretical development length value of 56.4 mm, as calculated in Equation 7.

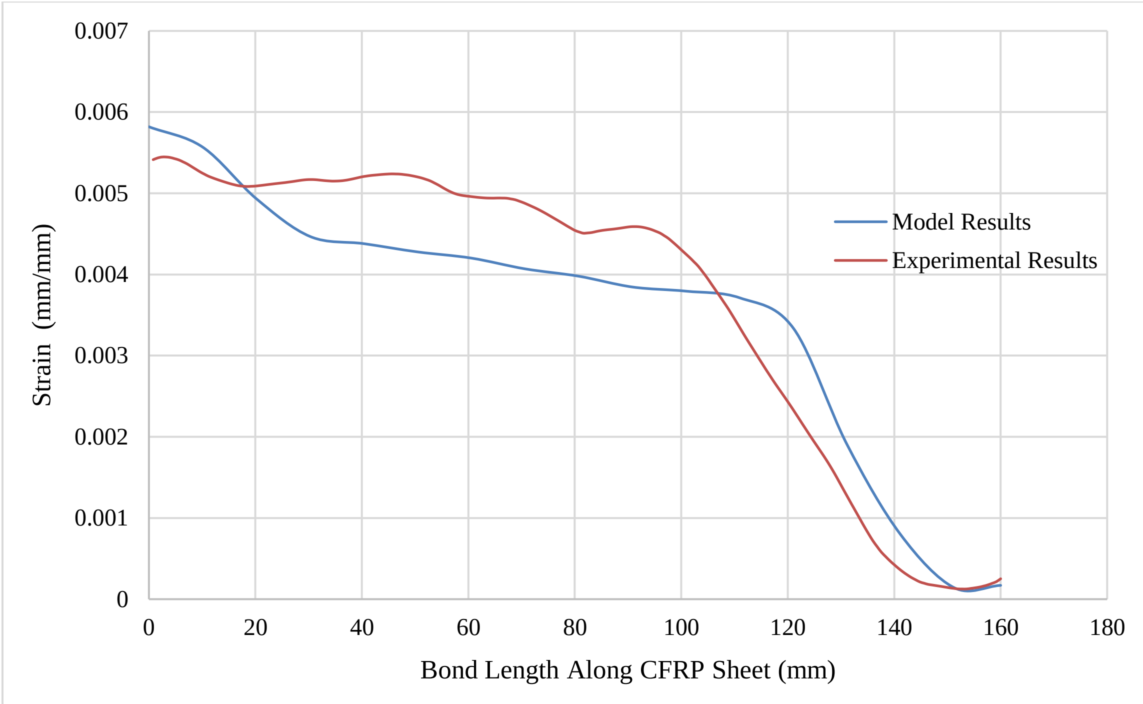

Figure 6.8. Strain vs. Bond Length Along CFRP Sheet Result Comparison

The following table provides a summary of the finite element model results in comparison to the experimental results, as discussed above.

Table 6.2. Summary of Model Results vs Experimental Results

Result Type	Maximum Load	Maximum Strain (mm/mm)	Development Length
ABAQUS Model	49.0 kN	0.0058	37.4 mm
Experimental Study [1]	41.5 kN	0.0054	40.0 mm
% Difference	16.57 %	7.14 %	6.72 %

Notes:

[1] The experimental study results are based on Atunbi's [35] L160-S-4 specimen.

7.0 CONCLUSIONS AND RECOMMENDATIONS

7.1 General

This project presents the numerical modelling of CFRP sheets externally bonded to reinforced concrete. The finite element model was to be constructed to simulate a previously completed experimental study performed in a laboratory at the University of New Brunswick. The main objective of this project was to investigate the effects of bond length on the development length and ultimate capacity of the CFRP sheet. Furthermore, the objective was to determine the model's level of accuracy by comparing results with the experimental study. The results of the numerical models lead to a number of conclusions, which include:

- ABAQUS is an appropriate finite element software to model CFRP sheets externally bonded to reinforced concrete.
- Detailed results with relative accuracy were obtained using ABAQUS when compared to the experimental results.
- Failure of the models was due to debonding of the CFRP sheet from the concrete.
- Results showed that an increase in bond length does not increase the development length (effective length) or the load capacity of the CFRP sheet.
- Calculated development lengths from the models underestimated the lengths when compared to the theoretical values.
- The 240 mm and 350 mm bond length models overpredicted the maximum tensile strain when compared to the theoretical value.

7.2 Limitations

When discussing limitations, the focus is centered on the finite element modelling. A brief summary of the identified limitations of this project can be found in the list below.

- The available experimental data that is relevant to the material properties and behaviour within ABAQUS is minimal. Although there are plenty of acceptable values that were used throughout the analysis, additional properties derived from the actual experiment is ideal.
- The reinforcing steel rebar was constrained to the concrete beam using a tie constraint, rather than a typical embedment constraint. This is due to the fact that only a quarter of the beam was modelled for the analysis. Furthermore, the experimental test setup applied the displacement load to the protruding rebar on each end. An embedded constraint would result in in a more typical behaviour between the concrete and rebar.
- The CFRP sheet and epoxy were modelled as one single element, rather than two. This was due to available input parameters from experimental testing as well as the complexity that comes when modelling cohesive elements. In an ideal scenario, the epoxy would be modelled as a separate cohesive element, resulting in a better representation of the material.
- In ABAQUS, each model was subjected to a 0.5 mm/min loading, which was done in replication of the experimental study. Figure 6.7 shows that the force curve of the experimental study is much smoother in comparison to the ABAQUS model results. Ideally, more investigation into the initial loading of the ABAQUS model should have been done in order to determine if the force curve could be more linear and consistent with the experimental study.

7.3 Recommendations

Upon completion of this research project, there a several recommendations that will be made regarding future work in this area. The following list provides a summary of them.

- Conduct additional testing in the laboratory to further investigate material properties that are required during a finite element model construction, mainly including the properties of the CFRP sheet and epoxy. This can be accomplished by exploring the input parameters and specifics of the software prior to conducting any experimental testing.
- Future work should carry out separate modelling parts for the CFRP sheet and epoxy with an unperfect bond. Although this may relate to the previous point of additional experimental work, modelling the cohesive epoxy layer as its own part will give the researcher a better insight into the bond behaviour at the CFRP-concrete interface.
- Incorporating different types of epoxies with varying properties should be considered. Along with this, consideration towards different types of FRPs, such as glass, aramid, and basalt, should be explored.

8.0 BIBLIOGRAPHY

[1] Y. N. Ziraba and M. H. Baluch, "Computational model for reinforced concrete beams strengthened by epoxy bonded steel plates," *Finite Elements in Analysis and Design*, vol. 20, pp. 253-271, 1995.

[2] M. A. Masuelli, "Introduction of Fibre-Reinfoced Polymers - Polymers and Composites: Concepts, Properties and Processes," in *Fibre Reinforced Polymers: The Technology Applied for Concrete Repair*, Rijeka, Croatia, InTech, 2012, pp. 3-40.

[3] G. M. Chen, J. G. Teng, J. F. Chen and Q. G. Xiao, "Finite element modeling of debonding failures in FRP-strengthened RC beams: A dynamic approach," *Computers and Structures,* vol. 158, pp. 167-183, 2015.

[4] S. Liu, W. Sun, H. Jing and Z. Dong, "Debonding detection and monitoring for CFRP reinforced concrete beams using pizeoceramic sensors," *Materials,* vol. 12, no. 13, 2019.

[5] S. S. Zhang and J. G. Teng, "Finite element analysis of end cover separation in RC beams strengthened in flexure with FRP," *Engineering Structures,* vol. 75, pp. 550-560, 2014.

[6] M. Barbato, "Efficient finite element modelling of reinforced concrete beams retrofitted with fibre reinforced polymers," *Computer and Structures,* vol. 87, pp. 167-176, 2009.

[7] F. Ascione, V. P. Berardi, L. Feo and A. Giordano, "An experimental study on the long-term behavior of CFRP pultruded laminates suitable to concrete structures rehabilitation," *Composites: Part B*, vol. 39, pp. 1147-1150, 2008.

[8] A. M. Carvajal, R. Vera, F. Corvo and A. Castañeda, "Diagnosis and rehabilitation of real reinforced concrete structures in coastal areas," *Corrosion Engineering, Science and Technology,* vol. 47, pp. 70-77, 2012.

[9] C.-K. Ma, N. M. Apandi, S. C. S. Yung, N. J. Hau, W. H. Lo, A. Z. Awang and W. Omar, "Repair and rehabilitation of concrete structures using confinement: A review," *Construction and Building Materials*, vol. 133, pp. 502-515, 2017.

[10] Horse Construction Co., Ltd., "Reinforcement of brick columns by steel jacketing," 2019. [Online]. Available: https://www.horseen.com/solution/reinforcement-brick-columns-steel-jacketing?page=5. [Accessed August 2019].

[11] ACI Committee 440, "Guide for the Design and Construction of Externally Bonded FRP Systems for Strengthening Concrete Structures (ACI 440.2R-08)," American Concrete Institute, Farmington Hills, MI, 2008.

[12] A. K. Kaw, Mechanics of Composite Materials, 2nd ed., Boca Raton, FL: Taylor & Francis Group, 2016.

[13] K. T. Chan, H. K. Cheong and D. M. Nguyen, "Experimental investigation on delamination failure of CFRP strenghtened beams," in *ICCMC/IBST 2001*

International Conference on Advanced Technologies in Design, Construction and Maintenance of Concrete Structures, 2001.

[14] S&P Clever Reinforcement Company AG, "S&P FRP Systems," S&P International, 2020. [Online]. [Accessed August 2019].

[15] B. Benmokrane, P. Wang, T. M. Ton-That, H. Rahman and J.-F. Robert, "Durability of Glass Fiber-Reinforced Polymer Reinforcing Bars in Concrete Environment," *Journal of Composites for Construction*, pp. 143-153, 2002.

[16] B&B FRP Manufacturing Inc., "MST-BAR GFRP Reinforcement," 2018. [Online]. Available: https://www.bandbfrp.com/mstbar. [Accessed 2020 May].

[17] I. Djafar-Henni and A. Kassoul, "Stress-strain model of confined concrete with Aramid FRP wraps," *Construction and Building Materials*, vol. 186, pp. 1016-1030, 2018.

[18] D. Tomlinson and A. Fam, "Performance of Concrete Beams Reinforced with Basalt FRP for Flexure and Shear," *Journal of Composites for Construction*, vol. 19, 2015.

[19] Smarter Building Systems, "Basalt Volcanic Composites," [Online]. Available: https://basalt.guru/smarter-building-systems/wp-content/uploads/sites/9/2014/08/SBS-Basalt-101.pdf. [Accessed September 2019].

[20] G. Wu, Z. Y. Sun, Z. S. Wu and Y. B. Luo, "Mechanical Properties of Steel-FRP Composite Bars (SFCBs) and Performance of SFCB Reinforced Concrete Structures," *Advances in Structural Engineering,* vol. 15, pp. 625-635, 2012.

[21] L. Tong, A. P. Mouritz and M. K. Bannister, 3D Fibre Reinforced Polymer Composites, Kidlington, Oxford: Elsevier, 2002.

[22] H. Hojo, K. Tsuda and K. Ogasawara, "Form and rate of corrosion of corrosion-resistant FRP resins," *Advanced Composite Materials,* vol. 1, pp. 55-67, 1991.

[23] M. Frigione and M. Lettieri, "Durability Issues and Challenges for Material Advancements in FRP Employed in the Construction Industry," *Polymers,* vol. 10, 2018.

[24] M. S. Sciolti, M. Frigione and M. A. Aiello, "Wet Lay-Up Manufactured FRPs for Concrete and Masonry Repair: Influence of Water on the Properties of Composites and on Their Epoxy Components," *Journal of Composites for Construction*, vol. 14, pp. 823-833, 2010.

[25] Lomon Molding LLC, "Thermoplastic Resin," Lomont Molding LLC, 2020. [Online]. Available: https://www.lomont.com/thermoplastic-resins. [Accessed January 2020].

[26] M. T. Arruda, J. P. Firmo, J. R. Correia and C. Tiago, "Numerical modelling of the bond between concrete and CFRP laminates at elevated temperatures," *Engineering Structures,* vol. 110, pp. 233-243, 2016.

[27] S. Cui, J. Wang, L. Shi and Y. Liu, "Test and FEM Analysis of Debonding Failure of RC Beam Strengthened with CFRP," *Reinforced Plastics and Composites,* vol. 28, pp. 2151-2160, 2009.

[28] J. M. Tripi, C. E. Bakis, T. E. Boothby and A. Nanni, "Deformation in Concrete with External CFRP Sheet Reinforcement," *Journal of Composites for Construction,* vol. 4, pp. 85-94, 2000.

[29] Horse Construction Co., Ltd., "200GSM CFRP Wrap," 2019. [Online]. Available: https://www.horseen.com/carbon-fiber-strengthening-system/unidirectional-CFRP-wrap. [Accessed July 2019].

[30] Canadian Standards Association, Design and construction of building structures with fibre-reinforced polymers, Mississauga, Ontario: Canadian Standards Association, 2012.

[31] CivilArc, "Carbon Fibre Reinforced Polymers (CFRP) Strengthening - NSMR," 23 January 2017. [Online]. Available: http://civilarc.com/carbon-fibre-reinforced-polymers-cfrp-strengthening-nsmr/. [Accessed September 2019].

[32] A. Gartner, E. P. Douglas, C. W. Dolan and H. R. Hamilton, "Small Beam Bond Test Method for CFRP Composites Applied to Concrete," *Journal of Composites for Construction*, vol. 15, pp. 52-61, 2011.

[33] D. M. Nguyen, T. K. Chan and H. K. Cheong, "Brittle Failure and Bond Development Length of CFRP-Concrete Beams," *Journal of Composites for Construction,* vol. 5, pp. 12-17, 2001.

[34] A. Hosseini and D. Mostofinejad, "Effective bond length of FRP-to-concrete adhesively-bonded joints: Experimental evaluation of existing models," *International Journal of Adhesion & Adhesives*, vol. 48, pp. 150-158, 2014.

[35] E. O. Atunbi, "Experimental Study on Bond Behaviour of CFRP Sheets Externally Bonded to Reinforced Concrete," University of New Brunswick, Fredericton, NB, 2018.

[36] J. F. Chen and J. G. Teng, "Anchorage Strength Models for FRP and Steel Plates Bonded to Concrete," *Structural Engineering*, vol. 127, pp. 784-791, 2001.

[37] J. G. Teng, L. De Lorenzis, B. Wang, R. Li, T. N. Wong and L. Lam, "Debonding Failures of RC Beams Strengthened with Near Surface Mounted CFRP Strips," *Journal of Composites for Construction*, vol. 10, pp. 92-105, 2006.

[38] H. Toutanji, L. Zhao and Y. Zhang, "Flexural behaviour of reinforced concrete beams externally strengthened with CFRP sheets bonded with an inorganic mix," *Engineering Structures,* vol. 28, pp. 557-566, 2006.

[39] J. A. O. de Barros and J. M. de Sena Cruz, "Bond Between Near-Surface Mounted Carbon-Fiber-Reinforced Polymer Laminate Strips and Concrete," *Journal of Composites for Construction,* vol. 8, pp. 519-527, 2004.

[40] Y. T. Obaidat, S. Heyden and O. Dahlblom, "The effect of CFRP and CFRP/concrete interface models when modelling retrofitted RC beams with FRM," *Composite Structures,* vol. 92, pp. 1391-1398, 2010.

[41] H. Al-Zubaidy, R. Al-Mahaidi and X.-L. Zhao, "Finite element modelling of CFRP/steel double strap joints subjected to dynamic tensile loadings," *Composite Structures,* vol. 99, pp. 48-61, 2013.

[42] G. M. Chen, J. F. Chen and J. G. Teng, "On the finite element modelling of RC beams shear-strengthened with FRP," *Construction and Building Materials,* vol. 32, pp. 13-26, 2012.

[43] R. de Borst, J. J. Remmers, A. Needleman and M.-A. Abellan, "Discrete vs smeared crack models for concrete fracture: bridging the gap," *International Journal for Numerical and Analytical Methods in Geomechanics,* vol. 28, pp. 583-607, 2004.

[44] Simulia, "Abaqus 6.13: Analysis User's Guide," Dassault Systemes, 2013. [Online]. Available: http://dsk.ippt.pan.pl/docs/abaqus/v6.13/. [Accessed January 2020].

[45] Y. Sumer and M. Aktas, "Defining parameters for concrete damage plasticity model," *Challenge Journal of Structural Mechanics,* vol. 1, no. 3, pp. 149-155, 2015.

[46] A. S. Genikomsou and M. A. Polak, "Damaged Plasticity Modelling of Concrete in Finite Element Analysis of Reinforced Concrete Slabs," in *9th International Conference on Fracture Mechanics of Concrete and Concrete Structures*, Berkeley, USA, 2016.

[47] Master Builders Solution by BASF, "MasterBrace FIB 300/50CFS," BASF Corporation, Shakopee, MN, 2019.

[48] "Digital Image Correlation (DIC)," Dantec Dynamics, 2019. [Online]. Available: https://www.dantecdynamics.com/digital-image-correlation. [Accessed January 2020].

[49] Correlated Solutions, "The VIC-3D 8 System," Correlated Solutions, Inc., 2020. [Online]. Available: https://www.correlatedsolutions.com/vic-3d/. [Accessed January 2020].

[50] O. de Weck and I. Y. Kim, "Finite Element Method," Massachusetts Institute of Technology, 2004.

[51] O. C. Zienkiewicz, R. L. Taylor and J. Z. Zhu, The Finite Element Method: Its Basis & Fundamentals, Kidlington, Oxford: Butterworth-Heinemann, 2013.

[52] Autodesk, "Finite Element Analysis," Autodesk Inc., 2020. [Online]. Available: https://www.autodesk.ca/en/solutions/finite-element-analysis. [Accessed January 2020].

[53] Simulia, "Abaqus Unified FEA," Dassault Systemes, 2020. [Online]. Available: https://www.3ds.com/products-services/simulia/products/abaqus/. [Accessed 2020 January].

[54] Ansys, "About Ansys," Ansys Inc, 2020. [Online]. Available: https://www.ansys.com/about-ansys. [Accessed January 2020].

[55] LS-DYNA, "About," Livermore Software Technology, 2019. [Online]. Available: https://www.lstc.com/products/ls-dyna. [Accessed 2020 January].

[56] MSC Software, "MSC Nastran: Multidisciplinary Structural Analysis," Hexagon, 2020. [Online]. Available: https://www.mscsoftware.com/product/msc-nastran. [Accessed January 2020].

[57] Altair Engineering, "Altair HyperMesh," Altair Engineering, Inc., 2020. [Online]. Available: https://www.altair.com/hypermesh/. [Accessed January 2020].

[58] P. H. Bischoff, "CE 3053: Reinforced Concrete Design I," University of New Brunswick, Fredericton, NB, 2016.

[59] MIT, "Module 3. Constitutive Equations," Massachusetts Institute of Technology, Cambridge, MA.

[60] SGI, "Hardened Concrete: Lecture No. 14," Sanjay Ghodawat Group of Insitutions, Maharashtra, India.

[61] Wikipedia, "Deformation (engineering)," March 2008. [Online]. Available: https://commons.wikimedia.org/wiki/File:Stress_Strain_Ductile_Material.png. [Accessed 2019 November].

[62] A. I. Karakas and A. T. Daloglu, "Shear and Volumetric Locking Effect on the Performance of Harmonic Solid Ring Finite Elements," *International Journal of Engineering & Applied Sciences,* vol. 7, pp. 68-85, 2015.

[63] Simulia, "Abaqus 6.14 Analysis User's Guide," Dassault Systemes, Providence, RI, 2014.

Curriculum Vitae

Candidate's full name:	Adam John Lawlor
Universities attended:	University of New Brunswick, B.Sc.E. (Civil Engineering), 2012-2016
Publications:	N/A
Conference Presentations:	N/A